Steady-state solutions in a three-dimensional nonlinear pool-boiling heat-transfer model

Michel Speetjens[*], Arnold Reusken[*†], Wolfgang Marquardt[‡]

RWTH Aachen, Templergraben 55, D-52056 Aachen, Germany.

Abstract

We consider a relatively simple model for pool-boiling processes. This model involves only the temperature distribution within the heater and describes the heat exchange with the boiling medium via a nonlinear boundary condition imposed on the fluid-heater interface. This results in a standard heat-transfer problem with a nonlinear Neumann boundary condition on part of the boundary. In a recent paper [18] we analysed this nonlinear heat-transfer problem for the case of *two space dimensions* and in particular studied the qualitative structure of steady-state solutions. The study revealed that, depending on system parameters, the model allows both multiple homogeneous and multiple heterogeneous temperature distributions on the fluid-heater interface. In the present paper we show that the analysis from Speetjens *et al.* [18] can be generalised to the physically more realistic case of *three space dimensions*. A fundamental shift-invariance property is derived that implies multiplicity of heterogeneous solutions. We present a numerical bifurcation analysis that demonstrates the multiple solution structure in this mathematical model by way of a representative case study.

Keywords: pool boiling, nonlinear heat transfer, bifurcations, numerical simulation

1 Introduction

Pool boiling refers to boiling processes that lean on natural convection as means for heat transfer through the boiling medium and is the key mode of thermal transport in many practical applications. Local heat-transfer phenomena near heating walls in industrial boiling equipment (e.g. evaporators and kettle reboilers) for instance are essentially pool-boiling processes [20]. Furthermore, pool boiling is emerging as novel cooling technique for electronics components [14]. Despite its importance, many aspects of (pool) boiling remain largely unexplored to date, mainly due to the immense complexity of the process induced by the intricate interplay between hydro- and thermodynamics. Studies on boiling known in the literature are mainly experimental and empirical. Theoretical investigations are scarce. The

[*]Chair of Numerical Analysis

[†]Corresponding author: Chair of Numerical Analysis, RWTH Aachen, Templergraben 55, D-52056 Aachen, Germany, +49-241-80-97973, reusken@igpm.rwth-aachen.de

[‡]Chair of Process Systems Engineering

theoretical analysis presented in this paper is intended to contribute to a better understanding of fundamental phenomena in pool boiling.

In pool boiling there are three fundamental states, namely nucleate, transition and film boiling, that occur successively with increasing temperature [6]. Nucleate boiling is, as opposed to film boiling, an efficient and safe mode of heat transfer and the sought-after state in typical applications. Nucleate boiling transits into film boiling upon exceeding the so-called critical heat flux (CHF) through the intermediate state of transition boiling. This transition results in a dramatic increase in interface temperature due to the substantial drop in the heat-transfer coefficient when going from nucleate boiling (homogeneous liquid-like mixture) to film boiling (vapour blanket on the interface). This manifests itself in the essentially nonlinear relation between the mean heat flux and the mean fluid-heater interface temperature (the so-called boiling curve; see [6]). Improvement of boiling processes involves finding a good balance between high efficiency (close to CHF) and low risk (safe distance from CHF). In-depth understanding of transition boiling and its underlying mechanisms is imperative to this [19].

Transition boiling has been interpreted as a boiling mode with coexisting nucleate boiling and film boiling regions ("two-mode boiling") and thus resulting essentially in a heterogeneous state at the surface (see e.g. [5]). A more intricate and most likely more precise description of the two-phase structure in transition boiling has been derived in a series of papers by Auracher and co-workers (see [2] for a survey). Moreover, transition boiling is an inherently unstable state that naturally evolves towards one of the two stable boiling modes, i.e. nucleate or film boiling, unless actively stabilised through temperature control [1]. On mesoscopic length and time scales two-mode boiling states correspond to heterogeneous temperature fields on the interface: "lower" temperatures correspond to nucleate-boiling regions; "higher" temperatures are associated with film-boiling regions.[1] The propagation of boundaries between adjacent boiling regions during evolution of the transition mode towards one of the stable modes is consistent with the propagation of thermal waves at the fluid-heater interface [21]. This phenomenological connection between a (mesoscopic) boiling mode and interface temperature admits a heater-only modelling approach that leaves out the boiling medium and describes the (qualitative) behaviour of the boiling system entirely in terms of the temperature distribution within the heater. This leads to a *nonlinear heat-transfer model* in terms of which fundamental (mesoscopic) boiling phenomena are analysed by means of numerical simulation.

This approach has found widespread application for the analysis of pool boiling on "thin" heaters (essentially wires and foils), cf. [7, 10, 11, 12, 21, 22]. In such thin configurations, which correspond to *spatially one-dimensional* (1D) models, the heat-flux relation leads to a source term in the governing equation, resulting in a model that is very similar to those used for describing reaction-diffusion systems [3]. First extensions to finite-thickness heaters, using a *spatially two-dimensional* (2D) model, have been presented in [3].

The transition behaviour of the heater-only problem basically involves two issues: (i) formation and (ii) dynamics of heterogeneous temperature fields [2]. These two issues lead to questions concerning existence and stability of steady-state solutions. Analysis of thin heaters has shown the existence of *multiple* steady-state solutions for given heating conditions. In [18] an extensive analysis of the steady-state behaviour of a *spatially 2D* heater problem is presented. The heat-transfer model used there is taken from [3]. In [18] it is shown

[1] Here mesoscopic means locally averaged in space and time over intervals larger than bubble dimensions and bubble lifetimes in order to smooth out microscopic short-term fluctuations [16].

that multiple steady-state solutions occur for specific heating conditions in this model. A main topic there is the analysis of the dependence of the multiple solution structure on the system parameters. To this end a bifurcation analysis of the governing mathematical model is performed in order to identify solution branches and bifurcations as a function of the system parameters.

In the present paper we generalise the analysis of the 2D pool-boiling problem in [18] to the physically more realistic *spatially three-dimensional* (3D) pool-boiling problem. An outline of our approach is as follows. The separation-of-variables method admits an analytical reduction of the 3D steady-state heat-transfer model to a 2D problem for the temperature distribution on the fluid-heater interface only. We apply a Fourier analysis to characterise the solutions of the reduced 2D problem. A shift-invariance property is proven, which implies multiplicity of heterogeneous solutions and reveals a symmetry structure of these multiple solutions. To be able to compute these multiple solutions we apply a discretisation and continuation technique. For the discretisation of the 2D reduced problem a standard Fourier collocation method has been employed. Continuation is performed for an artificial nonlinearity parameter λ in the Neumann boundary condition at the interface that enables control of the degree of nonlinearity of the system. This nonlinearity parameter ranges from $\lambda = 0$ (linear boundary condition and thus a linear problem) to $\lambda = 1$ (the actual nonlinear model) and enables systematic isolation of (multiple) solutions for given physical system parameters. Continuation in λ reveals that pitchfork bifurcations occur on a branch of homogeneous (i.e. constant interface temperature) solutions. These bifurcations occur for those λ at which the Jacobian of the governing nonlinear operator becomes singular and lead to multiple heterogeneous (i.e. non-constant interface temperature) solutions that have the symmetry property predicted by the theoretical analysis.

Although the topic considered is very similar to the one in the previous study [18], there are significant differences between the present and the previous paper. We mention the most important ones. In this paper we analyse the more realistic spatially *three*-dimensional heater. Due to this, the analysis becomes much more technical. In [18] the analysis and numerical methods are based on one-dimensional Fourier expansions, whereas in this paper we need two-dimensional Fourier series. It turns out that in the three-dimensional boiling model considered in this paper multi-dimensional kernels of the Jacobian can occur which cause special bifurcation phenomena. In the 2D case treated before the kernels are always one-dimensional. In [18] we present an extensive analysis in which many model parameters are varied and corresponding bifurcation diagrams are derived. In the present paper we investigate only one model problem in which all model parameters are fixed. A bifurcation diagram for only one (artificial) nonlinearity parameter is derived and analyzed.

The paper is organised as follows. In Section 2 we present the three-dimensional nonlinear heat-transfer model. In Section 3 we show how this 3D model leads to a reduced two-dimensional problem for the temperature profile at the interface. We derive important properties of this reduced problem. The discretisation method and the continuation technique for the reduced problem are explained in Section 4. In Section 5 we apply these methods to a representative case study and show results of a bifurcation analysis. A few main conclusions are summarised in Section 6.

2 Mathematical model for pool boiling

2.1 Dimensional heater-only model

Our pool boiling analysis is based on the heater-only modelling approach introduced in Section 1 and following [3]. We consider the three-dimensional rectangular heater $\mathcal{D} = [0, L] \times [0, W] \times [0, H]$, with boundary $\Gamma = \partial\mathcal{D} = \Gamma_H \cup \Gamma_A \cup \Gamma_F$. The boundary segments are $\Gamma_H = \{(x, y, z) \in \mathcal{D} \mid z = 0\}$ (heat supply), $\Gamma_A = \{ (x, y, z) \in \mathcal{D} \mid x \in \{0, L\} \text{ or } y \in \{0, W\} \}$ (adiabatic sidewalls) and $\Gamma_F = \{(x, y, z) \in \mathcal{D} \mid z = H \}$ (fluid-heater interface), cf. Figure 1*a*. The heat transfer is described in terms of the superheat $T = T_a - T_S$, i.e. the temperature difference between actual temperature T_a and a boiling point T_S, fixed by the pressure of the boiling fluid. The temperature distribution $T(\boldsymbol{x}, t)$ in $\mathcal{D} \times [0, t_{\text{end}}]$ is governed by the heat equation

$$\frac{\partial T}{\partial t} = \alpha \Delta T \qquad \text{in } \mathcal{D} \times [0, t_{\text{end}}], \qquad \alpha = \frac{\lambda}{\rho c_p}, \tag{1}$$

$$-\lambda \frac{\partial T}{\partial n}|_{\Gamma_H} = \bar{q}_H, \qquad -\lambda \frac{\partial T}{\partial n}|_{\Gamma_F} = \bar{q}_F(T_F), \qquad \frac{\partial T}{\partial n}|_{\Gamma_A} = 0, \tag{2}$$

$$T(\boldsymbol{x}, 0) = T_0(\boldsymbol{x}) \qquad \text{for } \boldsymbol{x} \in \mathcal{D}, \tag{3}$$

where T_F denotes the interface temperature on the boundary segment Γ_F. The constants ρ, c_p and λ are density, specific heat and thermal conductivity of the heater, respectively. The corresponding thermal diffusivity is denoted by α; $\bar{q}_H$ and $\bar{q}_F$ represent the constant heat supply and the temperature-dependent heat transfer to the boiling medium, respectively.

Closure of the heat-transfer model requires specification of the heat-flux function $\bar{q}_F(T_F)$. The boiling curve [6] is not guaranteed to hold locally on the heater surface at any particular point in time, since it is obtained from experiments, which average over time and space in a certain experimental situation. However, if we pragmatically assume that either liquid or vapour is in contact with a certain point on the surface at a certain time, the local heat-transfer model is supposed to reflect heat-transfer correlations specific to liquid contact below some threshold of the local heater surface temperature and specific to vapour contact above this threshold. Since discontinuous heat-transfer correlations will not occur in practice, the discontinuity between these two heat-transfer modes will be mollified by some smooth transition. For simplicity, we identify $\bar{q}_F(T_F)$ with the global boiling curve. Such boiling curves are of the functional form sketched in Figure 1*b* and consist of three distinct regimes that each correspond to one of the boiling modes: nucleate boiling ($0 \le T \le T_C$); transition boiling ($T_C < T < T_M$); film boiling ($T \ge T_M$). Temperatures T_C and T_M coincide with the local maximum (Q_C; CHF) and minimum (Q_M; Leidenfrost point) heat fluxes, respectively. T_D is a typical temperature during transition boiling. An explicit expression for the relation $\bar{q}_F(T_F)$ is given below.

2.2 Non-dimensional formulation and boiling curve

We formulate the above heat-transfer problem in non-dimensional form through rescaling the relevant variables as $\boldsymbol{x}' = \boldsymbol{x}/L$, $T' = T/T_D$, $t' = t/\tau$, $q'_H = \bar{q}_H/Q_H$ and $q'_F = \bar{q}_F/Q_C$. Substitution into the governing equations and dropping primes yields the non-dimensional

model

$$\begin{aligned} \frac{\partial T}{\partial t} &= \mu \Delta T \qquad \text{in } \ \mathcal{D} \times [0, t_{\text{end}}/\tau] \ , \ \ \mathcal{D} := [0,1] \times [0, D_1] \times [0, D_2], \\ -\Lambda \frac{\partial T}{\partial z}|_{\Gamma_H} &= 1, \quad -\Lambda \frac{\partial T}{\partial z}|_{\Gamma_F} = \Pi_2 \, q_F(T_F), \quad \frac{\partial T}{\partial n}|_{\Gamma_A} = 0, \\ T(\boldsymbol{x}, 0) &= T_0(\boldsymbol{x}) \qquad \text{for } \ \boldsymbol{x} \in \mathcal{D}, \end{aligned} \tag{4}$$

with

$$\Lambda = \frac{\lambda T_D}{Q_H L}, \ \ \mu = \frac{\lambda \tau}{\rho c_p L^2}, \ \ D_1 = \frac{W}{L}, \ \ D_2 = \frac{H}{L}, \ \ \Pi_1 = \frac{Q_C}{Q_M}, \ \ \Pi_2 = \frac{Q_C}{Q_H}, \ \ \Pi_3 = \frac{T_C}{T_M}, \tag{5}$$

as corresponding non-dimensional parameters. Here Q_H is a fixed typical value for the heat supply; in the current case of a constant heat supply we use $Q_H = \bar{q}_H$. Note that $q_F = \bar{q}_F / Q_C$ is the normalised boiling curve (i.e. rescaled with Q_C instead of Q_H); the dimensionless interfacial heat flux in terms of Q_H is given by $\Pi_2 q_F(T_F)$. Figure 2 shows the non-dimensional heater configuration (panel *a*) and the corresponding normalised boiling curve $q_F(T_F)$ (panel *b*). Physical considerations suggest $\tau = \rho c_p H T_D / |Q_H - Q_C|$, which leads to $\Lambda D_2 / \mu = |1 - \Pi_2|$. Thus the model contains six independent system parameters. Parameters Λ and μ are the non-dimensional thermal conductivity and thermal diffusivity, respectively, and thus control the thermal properties of the heater. The parameter Π_2 is the non-dimensional CHF and its reciprocal $\Pi_2^{-1} = \bar{q}_H / Q_C$ the normalised heat supply, and controls the heating conditions.

The normalised boiling curve is of the form $q_F(T_F) = h(T_F) T_F$, with the temperature-dependent heat-transfer coefficient $h(T_F)$ given by

$$h(T_F) = C_D \left\{ F_1 - F_2 H(C_D T_F - 1) \right\}, \qquad H(\zeta) = \frac{1}{2} \left[\tanh\left(\frac{2\zeta}{W} \right) + 1 \right], \tag{6}$$

where $H(\zeta)$ is a smoothed version of the Heaviside function. The parameter W controls the width of the transition region (from $H = 0$ to $H = 1$) around $\zeta = 0$ and is specified *a-priori*. The coefficient C_D rescales the temperature such that the single deflection point of $q_F(T_F)$ coincides with $T_F = 1$. Its value is defined implicitly through

$$2 \frac{dH}{dT}(C_D - 1) + \frac{d^2 H}{dT^2}(C_D - 1) = 0,$$

and thus depends only on W. The coefficients F_1 and F_2 scale $q_F(T_F)$ such that the conditions

$$\dot{q}_F(T_{max}) = 0, \quad \dot{q}_F(T_{min}) = 0, \quad q_F(T_{max}) = 1, \quad q_F(T_{min}) = \Pi_1^{-1}, \tag{7}$$

are fulfilled, i.e. that the extrema of the normalised boiling curve are consistent with their dimensional counterparts. We use the notation $\dot{q}_F = dq_F/dT$. These conditions result for given W and Π_1 in four nonlinear equations for the four unknowns $(F_1, F_2, T_{min}, T_{max})$. (It can be shown that q_F according to (6) possesses a local maximum and minimum at $T_{max} < 1$ and $T_{min} > 1$, respectively.) The temperatures $T_{max}, 1, T_{min}$ are the non-dimensional counterparts to T_C, T_D, T_M; the heat fluxes $q_F = 1$ and $q_F = \Pi_1^{-1}$ are the normalised counterparts to the CHF (Q_C) and the Leidenfrost heat flux (Q_M), respectively. Figure 2*b* shows the boiling curve thus attained for $W = 1$ and $\Pi_1 = 4$. Note that a value for the parameter W implies a corresponding value for the parameter Π_3. The present boiling curve is a generalisation of that proposed in [3] in that here the transition width W is an additional system parameter. For $W \downarrow 0$ we obtain the boiling curve used in [3].

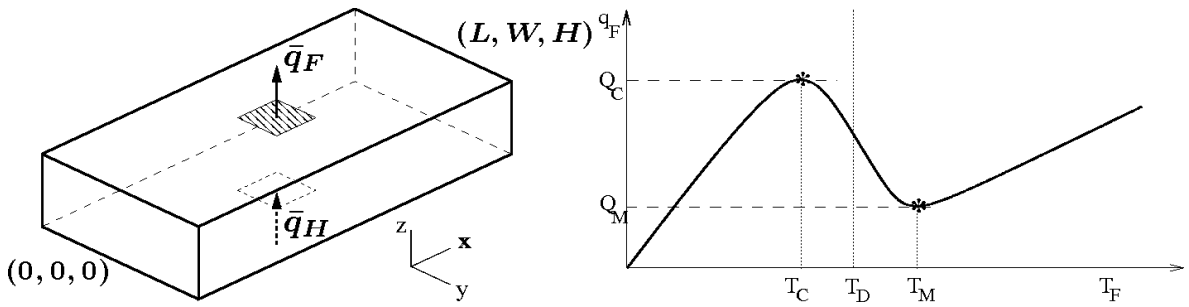

a) Heater configuration. *b) Boiling curve.*

Figure 1: *Heater configuration (panel a) and boiling curve (panel b). Temperatures T_C and T_M coincide with the local maximum (Q_C; CHF) and minimum (Q_M; Leidenfrost point) heat fluxes, respectively, and T_D is a typical temperature during transition boiling.*

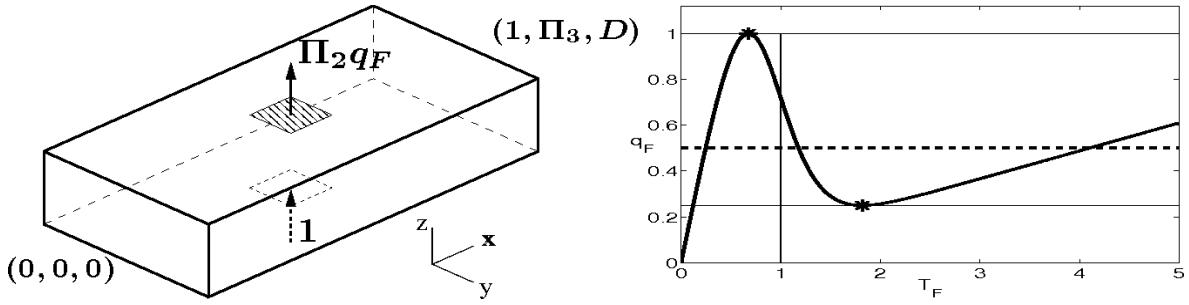

a) Heater configuration. *b) Normalised boiling curve.*

Figure 2: *Non-dimensional model: heater configuration (panel a) and normalised boiling curve for $\Pi_1 = 4$ and $W = 1$ (panel b). $T = 1$ is the non-dimensional counterpart to T_D; the extrema (stars) are the normalised CHF ($q_F = 1$) and Leidenfrost point ($q_F = \Pi_1^{-1}$). The dashed line represents the normalised heat supply $\bar{q}_H/Q_C = \Pi_2^{-1}$.*

3 Analysis of the steady-state heat-transfer problem

3.1 Reduced heat-transfer problem

We study the *steady-state* behaviour of the 3D nonlinear heat-transfer problem introduced above. Similar to the thin counterparts, the model (4) is expected to admit multiple steady-state solutions. We consider the corresponding steady-state heat-transfer problem

$$\begin{aligned} \Delta T = 0 \qquad & \text{in } \mathcal{D} = [0,1] \times [0, D_1] \times [0, D_2], \\ -\Lambda \frac{\partial T}{\partial z}|_{\Gamma_H} = 1, \qquad -\Lambda \frac{\partial T}{\partial z}|_{\Gamma_F} = \Pi_2 \, q_F(T_F), \qquad & \frac{\partial T}{\partial n}|_{\Gamma_A} = 0, \end{aligned} \tag{8}$$

with an associated set of parameters $(\Lambda, D_1, D_2, \Pi_1, \Pi_2, W)$. We apply the method of separation-of-variables (cf., for example, [13]) to derive a (formal) representation of the solution of the Laplace equation and the linear Neumann boundary conditions on Γ_H and Γ_A in (8). This

results in

$$T(x,y,z) = \sum_{n,p=0}^{\infty} \widetilde{T}_{n,p} \cos(n\pi x) \cos\left(\frac{p\pi y}{D_1}\right) \frac{\cosh(\kappa_{n,p}\pi z)}{\cosh(\kappa_{n,p}\pi D_2)} + \frac{D_2 - z}{\Lambda},$$
$$\kappa_{n,p} := \sqrt{n^2 + \left(\frac{p}{D_1}\right)^2}, \tag{9}$$

which can be checked by substitution. The coefficients $\widetilde{T}_{n,p}$ form the spectrum of the Fourier cosine expansion

$$T_F(x,y) := T(x,y,D_2) = \sum_{n,p=0}^{\infty} \widetilde{T}_{n,p} \cos(n\pi x) \cos\left(\frac{p\pi y}{D_1}\right), \tag{10}$$

of the interface temperature. The coefficients $\widetilde{T}_{n,p}$ are determined by the nonlinear Neumann boundary condition on Γ_F. Substitution of (9) into the nonlinear condition and using the relation $q_F(T_F) = h(T_F)T_F$ leads to

$$\sum_{n,p=0}^{\infty} \kappa_{n,p}\pi \tanh(\kappa_{n,p}\pi D_2) \widetilde{T}_{n,p} \cos(n\pi x) \cos\left(\frac{p\pi y}{D_1}\right) + \alpha(T_F(x,y))T_F(x,y) - \frac{1}{\Lambda} = 0, \tag{11}$$

for all $(x,y) \in \Gamma_F$, with

$$\alpha(T_F) = \frac{\Pi_2}{\Lambda} h(T_F) = \frac{\Pi_2}{\Lambda} \frac{q_F(T_F)}{T_F},$$

the scaled heat-transfer coefficient. The nonlinear equation (11) is the characteristic equation that determines the steady-state solutions of (8). The series in (10) and (11) are formal expressions. Convergence of these series is discussed below.

Thus the 3D steady-state problem (8) *simplifies to the 2D problem* (11) *involving only the temperature distribution* $T_F(x,y)$ *on the boundary* Γ_F.

We call the 2D problem (11) the *reduced* heat-transfer problem.

3.2 Solutions of the reduced heat-transfer problem

Homogeneous solutions

We first consider the special case of *homogeneous* interface temperatures T_F, implying $T_F(x,y) = \widetilde{T}_{0,0}$ and $\widetilde{T}_{n,p} = 0$ for all $(n,p) \neq (0,0)$. Then the characteristic equation (11) simplifies to

$$q_F(\widetilde{T}_{0,0}) = \Pi_2^{-1}, \tag{12}$$

and $\widetilde{T}_{0,0}$ coincides with the intersection(s) between boiling curve q_F and normalised heat-supply $\bar{q}_H/Q_C = \Pi_2^{-1}$ (dashed line in Figure 2*b*). From Figure 2*b* it follows that, depending on the system parameters Π_1 and Π_2, we can have one, two or three solutions for $\widetilde{T}_{0,0}$. Note that in this homogeneous case the heat-transfer coefficient $h(T_F)$ is constant and thus the Neumann boundary condition on Γ_F is linear. The corresponding solution in $\mathcal{D}$ is given by

$$T(x,y,z) = \frac{D_2}{\Lambda}\left(1 - \frac{z}{D_2}\right) + \widetilde{T}_{0,0}\ , \tag{13}$$

which is a linear temperature profile with the constant interface temperature $T(x,y,D_2) = T_F(x,y) = \widetilde{T}_{0,0}$ defined by (12).

Heterogeneous solutions

We now return to the general case and derive two properties that play an important role in the remainder of this paper. For this we introduce the following spaces of *convergent* double cosine Fourier series for $k, \ell \geq 1$:

$$V_{k,\ell} := \{\, g : \mathbb{R}^2 \to \mathbb{R} \mid g(x,y) = \sum_{n,p=0}^{\infty} a_{kn,\ell p} \cos(kn\pi x) \cos\Big(\frac{\ell p \pi y}{D_1}\Big) \quad \forall\ (x,y) \in \mathbb{R}^2 \,\}. \tag{14}$$

For the topic of convergence of bivariate Fourier series we refer to the literature, e.g., [8]. We also use spaces of Fourier univariate cosine series. For this it is convenient to use the following notation

$$V_{k,\infty} := \{\, g : \mathbb{R}^2 \to \mathbb{R} \mid g(x,y) = \sum_{n=0}^{\infty} a_{kn} \cos(kn\pi x) \quad \forall\ (x,y) \in \mathbb{R}^2 \,\}, \quad k \geq 1,$$

$$V_{\infty,\ell} := \{\, g : \mathbb{R}^2 \to \mathbb{R} \mid g(x,y) = \sum_{p=0}^{\infty} a_{\ell p} \cos\Big(\frac{\ell p \pi y}{D_1}\Big) \quad \forall\ (x,y) \in \mathbb{R}^2 \,\}, \quad \ell \geq 1.$$

Remark 1 For the analysis below it is helpful to have one notation that describes both the bivariate and univariate Fourier series. For a function $g \in V_{k,\ell}$ with $k < \infty$, $\ell = \infty$ we therefore introduce the notation

$$g(x,y) = \sum_{n=0}^{\infty} a_{kn} \cos(kn\pi x) =: \sum_{n,p=0}^{\infty} a_{kn,\ell p} \cos(kn\pi x) \cos\Big(\frac{\ell p \pi y}{D_1}\Big),$$
$$\text{with} \quad a_{kn,\ell p} := 0 \quad \text{for all} \quad p \geq 1, \quad a_{kn,\ell p} := a_{kn} \quad \text{for} \quad p = 0.$$

Similarly for $\ell < \infty$, $k = \infty$.

Functions from the space $V_{k,\ell}$ are $\frac{2}{k}$-periodic in x, $\frac{2D_1}{\ell}$-periodic in y (with $\frac{c}{\infty}$-periodic:=constant) and even: $g(x,y) = g(-x,y) = g(x,-y)$. Such functions are uniquely determined by their values at $(x,y) \in [0, \frac{1}{k}] \times [0, \frac{D_1}{\ell}]$ (with $\frac{c}{\infty} := 0$). For $1 \leq k, \ell < \infty$, the inclusions $V_{\infty,\ell} \subset V_{2k,\ell} \subset V_{k,\ell}$, $V_{k,\infty} \subset V_{k,2\ell} \subset V_{k,\ell}$ and $V_{k,\ell} \subset V_{1,1}$ hold. In the bivariate case the Fourier coefficients have the following representation for $kn > 0, \ell p > 0$:

$$a_{kn,\ell p} = \frac{4}{D_1} \int_0^{D_1} \int_0^1 g(x,y) \cos(kn\pi x) \cos\Big(\frac{\ell p \pi y}{D_1}\Big)\, dxdy,$$
$$a_{kn,0} = \frac{2}{D_1} \int_0^{D_1} \int_0^1 g(x,y) \cos(kn\pi x)\, dxdy,$$
$$a_{0,\ell p} = \frac{2}{D_1} \int_0^{D_1} \int_0^1 g(x,y) \cos\Big(\frac{\ell p \pi y}{D_1}\Big)\, dxdy,$$
$$a_{0,0} = \frac{1}{D_1} \int_0^{D_1} \int_0^1 g(x,y)\, dxdy.$$

The Fourier transform on $V_{1,1}$ is denoted by $\mathcal{F} : V_{1,1} \to \mathbb{R}^{\infty \times \infty}$:

$$\text{for} \quad g(x,y) = \sum_{n,p=0}^{\infty} a_{n,p} \cos(n\pi x) \cos\Big(\frac{p\pi y}{D_1}\Big), \quad \mathcal{F}(g) := (a_{n,p})_{n,p=0}^{\infty}. \tag{15}$$

Here $\mathbb{R}^{\infty\times\infty}$ denotes the space of infinite matrices with real entries. For $\mathbf{b} := (b_{n,p})_{n,p=0}^{\infty}$, $\mathbf{c} := (c_{n,p})_{n,p=0}^{\infty} \in \mathbb{R}^{\infty\times\infty}$ we define the Hadamard product $\mathbf{b} * \mathbf{c} := (b_{n,p}c_{n,p})_{n,p=0}^{\infty}$, i.e., elementwise multiplication of the entries in the matrices. In view of (11) we introduce the infinite matrix $\mathbf{d} = (d_{n,p})_{n,p=0}^{\infty}$ defined by

$$d_{n,p} := \kappa_{n,p}\pi \tanh(\kappa_{n,p}\pi D_2) \quad \text{for all} \;\; n,p \geq 0. \tag{16}$$

To guarantee that the expressions on the left handside in (11) are well-defined we only consider functions from the following subset of $V_{1,1}$:

$$S := \{\, g \in V_{1,1} \mid \mathbf{d} * \mathcal{F}(g) \in \mathrm{range}(\mathcal{F}) \;\; \text{and} \;\; (\alpha \circ g)g \in V_{1,1} \,\}.$$

Remark 2 Functions $g \in V_{1,1}$ that are *sufficiently smooth* are elements of S. We do not study this smoothness issue here. In our numerical simulations we always observed that the discrete solutions show exponential convergence to very smooth continuous functions that lie in S.

The operator on the left handside in (11) has the following form

$$\mathcal{G}(T_F) := \mathcal{F}^{-1}\big(\mathbf{d} * \mathcal{F}(T_F)\big) + (\alpha \circ T_F)T_F - \frac{1}{\Lambda}, \quad \text{for} \;\; T_F \in S. \tag{17}$$

From the definition of S it immediately follows that $\mathcal{G} : S \to V_{1,1}$. Thus (11) leads to the following problem:

$$\text{Determine } T_F \in S \text{ such that} \quad \mathcal{G}(T_F) = 0\,. \tag{18}$$

The operator $\mathcal{G}$, defined on S, is (strongly) nonlinear. The homogeneous solutions given by (12) satisfy $\mathcal{G}(\widetilde{T}_{0,0}) = 0$. We now show that for all $k,\ell \geq 1$ the range of $\mathcal{G}_{|V_{k,\ell}}$ is contained in $V_{k,\ell}$. Below we will see that due to this we have an important conservation-of-symmetry property in the continuation method.

Theorem 1 *The following holds:*

$$\mathcal{G} : V_{k,\ell} \cap S \to V_{k,\ell} \quad \textit{for all} \;\; k,\ell \geq 1.$$

Proof. For $k = \ell = 1$ this is trivial due to the definition of S. We consider $k < \infty$, $\ell < \infty$. The case $k = \infty$ or $\ell = \infty$ (i.e., univariate Fourier series) can be treated similarly and requires only notational modifications. Take $T_F \in V_{k,\ell} \cap S$. Then T_F can be represented as $T_F(x,y) = \sum_{n,p=0}^{\infty} \widetilde{T}_{kn,\ell p} \cos(kn\pi x) \cos\left(\frac{\ell p \pi y}{D_1}\right)$ and all Fourier coefficients $\widetilde{T}_{m,r}$ with $m \bmod k \neq 0$ or $r \bmod \ell \neq 0$ are equal to zero. We obtain

$$\begin{aligned}
\mathcal{G}(T_F)(x,y) &= \sum_{n,p=0}^{\infty} d_{n,p}\widetilde{T}_{n,p} \cos(n\pi x) \cos\left(\frac{p\pi y}{D_1}\right) + \alpha(T_F(x,y))T_F(x,y) - \frac{1}{\Lambda} \\
&= \sum_{n,p=0}^{\infty} d_{kn,\ell p}\widetilde{T}_{kn,\ell p} \cos(kn\pi x) \cos\left(\frac{\ell p\pi y}{D_1}\right) + \alpha(T_F(x,y))T_F(x,y) - \frac{1}{\Lambda} \\
&=: w_1(x,y) + w_2(x,y) - \frac{1}{\Lambda}.
\end{aligned}$$

From $T_F \in S$ it follows that the double series $w_1(x,y) = \sum_{n,p=0}^{\infty} d_{kn,\ell p} \widetilde{T}_{kn,\ell p} \cos(kn\pi x) \cos\left(\frac{\ell p \pi y}{D_1}\right)$ converges and thus $w_1 \in V_{k,\ell}$. From $T_F \in S$ it also follows that $w_2 = (\alpha \circ T_F) T_F \in V_{1,1}$ and thus w_2 has a convergent double cosine Fourier series. The function T_F is $\frac{2}{k}$-periodic in x and $\frac{2D_1}{\ell}$-periodic in y and thus $w_2 = (\alpha \circ T_F) T_F$ has the same properties. Hence, we have $w_2 \in V_{k,\ell}$. Thus we have $\mathcal{G}(T_F) = w_1 + w_2 - \frac{1}{\Lambda} \in V_{k,\ell}$. □

In the next theorem we present a main result, which shows that heterogeneous solutions, if they exist, are non-unique. For $\ell = \infty$ we use the notation as in Remark 1 and we set $\frac{1}{\ell} := 0$, similarly for $k = \infty$.

Theorem 2 *Assume that there exist* $1 \le k, \ell \le \infty$ *and* $T_F \in V_{k,\ell} \cap S$ *such that* $T_F \notin V_{k',\ell}$ *for* $k' > k$, $T_F \notin V_{k,\ell'}$ *for* $\ell' > \ell$, *and*

$$T_F(x,y) = \sum_{n,p=0}^{\infty} \widetilde{T}_{kn,\ell p} \cos(kn\pi x) \cos\Big(\frac{\ell p \pi y}{D_1}\Big), \tag{19}$$

satisfies $\mathcal{G}(T_F) = 0$. *Define*

$$T_F^{*,1}(x,y) := T_F(x + \frac{1}{k}, y) = \sum_{n,p=0}^{\infty} \widetilde{T}^{(1)}_{kn,\ell p} \cos(kn\pi x) \cos\Big(\frac{\ell p \pi y}{D_1}\Big), \tag{20}$$

$$T_F^{*,2}(x,y) := T_F(x, y + \frac{D_1}{\ell}) = \sum_{n,p=0}^{\infty} \widetilde{T}^{(2)}_{kn,\ell p} \cos(kn\pi x) \cos\Big(\frac{\ell p \pi y}{D_1}\Big), \tag{21}$$

$$T_F^{*,3}(x,y) := T_F(x + \frac{1}{k}, y + \frac{D_1}{\ell}) = \sum_{n,p=0}^{\infty} \widetilde{T}^{(3)}_{kn,\ell p} \cos(kn\pi x) \cos\Big(\frac{\ell p \pi y}{D_1}\Big), \tag{22}$$

with

$$\widetilde{T}^{(1)}_{kn,\ell p} = (-1)^n \widetilde{T}_{kn,\ell p}, \quad \widetilde{T}^{(2)}_{kn,\ell p} = (-1)^p \widetilde{T}_{kn,\ell p}, \quad \widetilde{T}^{(3)}_{kn,\ell p} = (-1)^{n+p} \widetilde{T}_{kn,\ell p}. \tag{23}$$

Then $T_F^{*,i} \in V_{k,\ell} \cap S$ *satisfies* $\mathcal{G}(T_F^{*,i}) = 0$ *for* $i = 1,2,3$. *Furthermore* $T_F^{*,i} \neq T_F$ *holds for* $i = 1$ *or* 2.

Proof. We consider $k < \infty$, $\ell < \infty$. The case $k = \infty$ or $\ell = \infty$ (i.e., univariate Fourier series) can be treated similarly and requires only notational modifications. Note that $T_F \in V_{k,\ell} \cap S$ is even in both variables, $\frac{2}{k}$-periodic in x and $\frac{2D_1}{\ell}$-periodic in y. The function $T_F^{*,i}$ is obtained from T_F by a translation with $\frac{1}{k}$ in x-direction and/or a translation with $\frac{D_1}{\ell}$ in y-direction. Hence, we have $T_F^{*,i} \in V_{k,\ell} \cap S$ for $i = 1,2,3$. For $i = 3$ we have

$$\begin{aligned} T_F(x + \frac{1}{k}, y + \frac{D_1}{\ell}) &= \sum_{n,p=0}^{\infty} \widetilde{T}_{kn,\ell p} \cos(kn\pi(x + \frac{1}{k})) \cos\Big(\frac{\ell p \pi (y + D_1/\ell)}{D_1}\Big) \\ &= \sum_{n,p=0}^{\infty} (-1)^{n+p} \widetilde{T}_{kn,\ell p} \cos(kn\pi x) \cos\Big(\frac{\ell p \pi y}{D_1}\Big), \end{aligned}$$

and thus we obtain the representation in (22). The cases $i = 1,2$ can be treated similarly to derive the representations in (20) and (21). We now show that $T_F^{*,1} \neq T_F$ holds. The

representations of T_F and $T_F^{*,1}$ yield

$$T_F(x,y) - T_F^{*,1}(x,y) = \sum_{n,p=0}^{\infty} (1-(-1)^n)\widetilde{T}_{kn,\ell p}\cos(kn\pi x)\cos\Big(\frac{\ell p\pi y}{D_1}\Big).$$

Assume that $T_F = T_F^{*,1}$ holds. Then $\widetilde{T}_{kn,\ell p} = 0$ must hold for all odd n, and thus we obtain the representation $T_F(x,y) = \sum_{n,p=0}^{\infty} \widetilde{T}_{2kn,\ell p}\cos(2kn\pi x)\cos\Big(\frac{\ell p\pi y}{D_1}\Big)$. This implies $T_F \in V_{2k,\ell}$, which contradicts the assumption $T_F \notin V_{k',\ell}$ for $k' > k$. Thus $T_F^{*,1} \neq T_F$ must hold. Similar arguments can be applied to show $T_F^{*,2} \neq T_F$. For $k = \infty$ ($\ell = \infty$) we have $T_F^{*,1} = T_F$, $T_F^{*,2} \neq T_F$ ($T_F^{*,2} = T_F$, $T_F^{*,1} \neq T_F$, respectively).
For arbitrary $(x,y) \in \mathbb{R}^2$ we have

$$\begin{aligned}
&\mathcal{G}(T_F^{*,1})(x,y)\\
&= \mathcal{F}^{-1}\big(\mathbf{d}\cdot\mathcal{F}(T_F^{*,1})\big)(x,y) + \alpha(T_F^{*,1}(x,y))T_F^{*,1}(x,y) - \frac{1}{\Lambda}\\
&= \sum_{n,p=0}^{\infty} d_{kn,\ell p}(-1)^n\widetilde{T}_{kn,\ell p}\cos(kn\pi x)\cos\Big(\frac{\ell p\pi y}{D_1}\Big) + \alpha(T_F^{*,1}(x,y))T_F^{*,1}(x,y) - \frac{1}{\Lambda}\\
&= \sum_{n,p=0}^{\infty} d_{kn,\ell p}\widetilde{T}_{kn,\ell p}\cos(kn\pi(x+\frac{1}{k}))\cos\Big(\frac{\ell p\pi y}{D_1}\Big) + \alpha(T_F^{*,1}(x,y))T_F^{*,1}(x,y) - \frac{1}{\Lambda}\\
&= \mathcal{F}^{-1}\big(\mathbf{d}\cdot\mathcal{F}(T_F)\big)(x+\frac{1}{k},y) + \alpha(T_F(x+\frac{1}{k},y))T_F(x+\frac{1}{k},y) - \frac{1}{\Lambda}\\
&= \mathcal{G}(T_F)(x+\frac{1}{k},y) = 0.
\end{aligned}$$

Hence, $\mathcal{G}(T_F^{*,1}) = 0$ holds. A very similar reasoning can be applied to prove that $\mathcal{G}(T_F^{*,i}) = 0$ holds for $i = 2, 3$, too. □

This result shows that heterogeneous solutions in $V_{1,1} \cap S$, if they exist, always induce three associated solutions, which we call *dual shifted* solutions. At least one of these three, namely (20) or (21) (which may be equal), differs from T_F. This implies a fundamental non-uniqueness in the steady states under heterogeneous boiling conditions, consistent with laboratory experiments [2]. Note that the dual shifted solutions $T_F^{*,i}$ are obtained from T_F by a translation with half the period of T_F. This implies certain symmetry relations between T_F and its dual shifted solutions.

In the proof of Theorem 2 we derived the following fundamental property of the operator $\mathcal{G} : V_{k,\ell} \cap S \to V_{k,\ell}$. For $i = 1, 2, 3$, let $s_i : \mathbb{R}^2 \to \mathbb{R}^2$ be the linear shift function $s_1(x,y) := (x + \frac{1}{k}, y)$, $s_2(x,y) := (x, y + \frac{D_1}{\ell})$, $s_3(x,y) := (x + \frac{1}{k}, y + \frac{D_1}{\ell})$. Note that $s_3 = s_1 \circ s_2 = s_2 \circ s_1$. For $T_F \in V_{k,\ell} \cap S$ the relations

$$\mathcal{G}(T_F \circ s_i) = s_i \circ \mathcal{G}(T_F), \quad i = 1, 2, 3, \tag{24}$$

hold. The relation for $i = 3$ is a direct consequence of the relations for $i = 1, 2$. Due to this commutator property of the nonlinear operator $\mathcal{G}$ and the linear shift operators s_i we obtain the non-uniqueness result in Theorem 2.

Remark 3 In the proofs of Theorem 1 and Theorem 2 we did not use any specific information about the form of the function $\alpha(\cdot)$. Thus these results hold for an arbitrary (smooth) boiling curve q_F.

In case of a square fluid-heater interface ($D_1 = 1$) a further multiplicity property, in addition to the one presented in Theorem 2, holds:

Lemma 1 *Assume $D_1 = 1$ (square fluid-heater interface). Let $T_F \in V_{k,\ell} \cap S$ be a solution to the reduced heat-transfer problem: $\mathcal{G}(T_F) = 0$. Then there exists a dual reflected solution $T'_F(x,y) := T_F(y,x)$ (with $\widetilde{T}'_{kn,\ell p} = \widetilde{T}_{\ell p,kn}$) that also satisfies the reduced heat-transfer problem: $\mathcal{G}(T'_F) = 0$.*

Proof. Using arguments as in the second part of the proof of Theorem 2 one can show that for arbitrary $(x,y) \in \mathbb{R}^2$:

$$\begin{aligned}\mathcal{G}(T'_F)(x,y) &= \mathcal{F}^{-1}\big(\mathbf{d}\cdot\mathcal{F}(T'_F)\big)(x,y) + \alpha(T'_F(x,y))T'_F(x,y) - \frac{1}{\Lambda}\\ &= \mathcal{F}^{-1}\big(\mathbf{d}\cdot\mathcal{F}(T_F)\big)(y,x) + \alpha(T_F(y,x))T_F(y,x) - \frac{1}{\Lambda}\\ &= \mathcal{G}(T_F)(y,x) = 0.\end{aligned}$$

□

4 Numerical solution method

A steady-state solution is obtained by solving the characteristic equation (11). For homogeneous solutions the latter simplifies to (12), which can easily be solved by a standard root-finding algorithm. Thus homogeneous solution branches corresponding to the system parameters are easily identified. Heterogeneous solutions are determined via a discretisation and continuation approach that is explained in this section. Numerical results obtained with this method are presented in Section 5.

4.1 Discretisation method

Discretisation of (11) is based on a standard Fourier collocation method [4]. We briefly review a few basic facts from discrete Fourier analysis. Consider for $N \in \mathbb{N}$ the equidistant mesh $x_j = j/N,\ j \in \mathbb{N}$. The discrete Fourier cosine transform of an even 2-periodic function $u(x) = u(x+2)$ is given by

$$u(x) = \sum_{n=0}^{N} \widetilde{u}_n \cos(n\pi x), \quad \widetilde{u}_n := \frac{c_n}{N}\Big\{u(0) + 2\sum_{j=1}^{N-1} u(x_j)\cos(n\pi x_j) + (-1)^n u(1)\Big\}, \quad (25)$$

with $c_0 = c_N = 1/2$ and $c_n = 1$ otherwise. This function satisfies

$$u(x_i) = \sum_{n=0}^{N} \widetilde{u}_n \cos(n\pi x_i) \quad \text{for all} \ \ 0 \le i \le N.$$

Hence, the (physical) values $\boldsymbol{u} = (u_0, \ldots, u_N)^T$, with $u_j := u(x_j)$, relate to the spectral coefficients $\widetilde{\boldsymbol{u}} = (\widetilde{u}_0, \ldots, \widetilde{u}_N)^T$ via

$$\boldsymbol{u} = \boldsymbol{V}_N \widetilde{\boldsymbol{u}}, \quad \mathbf{V}_N := \begin{bmatrix} 1 & \cos(\pi x_0) & \ldots & \cos(N\pi x_0) \\ \vdots & \vdots & & \vdots \\ 1 & \cos(\pi x_N) & \ldots & \cos(N\pi x_N) \end{bmatrix}. \tag{26}$$

An elementary computation yields

$$(\mathbf{V}_N \boldsymbol{D})^{-1} = \frac{2}{N} \mathbf{V}_N \boldsymbol{D}, \quad \text{with } \boldsymbol{D} = \operatorname{diag}(\frac{1}{2}, 1, \ldots, 1, \frac{1}{2}). \tag{27}$$

The above 1D Fourier representation of $u(x)$ readily extends to a 2D periodic function $u(x, y) = u(x + 2, y + 2D_1)$. For $N, P \in \mathbb{N}$ we introduce the equidistant mesh $(x_i, y_j) := \left(\frac{i}{N}, \frac{jD_1}{P}\right)$, with $i = 0, \ldots, N$ and $j = 0, \ldots, P$. The 2D Fourier finite cosine expansion of u is given by

$$u(x, y) \;=\; \sum_{n=0}^{N} \sum_{p=0}^{P} \widetilde{u}_{n,p} \cos(n\pi x) \cos\left(\frac{p\pi y}{D_1}\right). \tag{28}$$

The truncated expansion $u(x, y)$ is an approximation of the infinite Fourier expansion of functions $g(x, y) \in V_{1,1}$, cf. (14).

The Fourier coefficients $\tilde{u}_{n,p}$ in (28) are uniquely determined by the equations

$$u(x_i, y_j) = \sum_{n=0}^{N} \sum_{p=0}^{P} \widetilde{u}_{n,p} \cos(n\pi x_i) \cos\left(\frac{p\pi y_j}{D_1}\right), \quad 0 \le i \le N,\, 0 \le j \le P. \tag{29}$$

For a matrix representation of this we need some further notation. Let $\boldsymbol{U} \in \mathbb{R}^{(N+1)\times(P+1)}$ be the matrix with entries $u_{i,j} = u(x_i, y_j)$ (physical values) and $\tilde{\boldsymbol{U}} \in \mathbb{R}^{(N+1)\times(P+1)}$ the matrix with the Fourier coefficients $\tilde{u}_{n,p}$. Let $\mathbf{V}_P$ be the $(P + 1) \times (P + 1)$-matrix as in (26) but with $n\pi x_i$ replaced by $\frac{p\pi y_j}{D_1}$ $(0 \le p, j \le P)$. A simple computation shows that the system of equations in (29) can be represented as

$$\boldsymbol{U} = \mathbf{V}_N \, \widetilde{\boldsymbol{U}} \, \mathbf{V}_P^T. \tag{30}$$

Thus the Fourier coefficients are given by $\widetilde{\boldsymbol{U}} = \mathbf{V}_N^{-1} \, \boldsymbol{U} \, \mathbf{V}_P^{-T}$. Due to orthogonality the inverses follow explicitly from (27). This yields the discrete Fourier transform $\boldsymbol{\mathcal{F}} : \mathbb{R}^{N\times P} \to \mathbb{R}^{N\times P}$:

$$\boldsymbol{\mathcal{F}}(\boldsymbol{U}) = \boldsymbol{V}_N^{-1} \boldsymbol{U} \boldsymbol{V}_P^{-T}, \quad \boldsymbol{\mathcal{F}}^{-1}(\widetilde{\boldsymbol{U}}) = \boldsymbol{V}_N \widetilde{\boldsymbol{U}} \boldsymbol{V}_P^T, \tag{31}$$

as discrete counterpart of the continuous Fourier transform (15).

The discretisation of the characteristic equation (11) is as follows: determine $T_F(x_i, y_j) = \sum_{n=0}^{N} \sum_{p=0}^{P} \widetilde{T}_{n,p} \cos(n\pi x_i) \cos\left(\frac{p\pi y_j}{D_1}\right)$, $0 \le i \le N$, $0 \le j \le P$, such that

$$\sum_{n=0}^{N} \sum_{p=0}^{P} d_{n,p} \widetilde{T}_{n,p} \cos(n\pi x_i) \cos\left(\frac{p\pi y_j}{D_1}\right) + \alpha(T_F(x_i, y_j)) T_F(x_i, y_j) - \frac{1}{\Lambda} = 0, \tag{32}$$

for all $0 \le i \le N$, $0 \le j \le P$. Using matrix notation we can formulate this discrete nonlinear problem in a more compact form. We introduce the $N \times P$ matrices $\boldsymbol{T}_F$, $\boldsymbol{M}(\boldsymbol{T}_F)$, $\boldsymbol{G}$, $\tilde{\boldsymbol{T}}_F$ and $\boldsymbol{D}$ defined as follows:

$$(\boldsymbol{T}_F)_{i,j} = T_F(x_i, y_j), \quad \big(\boldsymbol{M}(\boldsymbol{T}_F)\big)_{i,j} = \alpha(T_F(x_i, y_j)), \quad \boldsymbol{G}_{i,j} = \frac{1}{\Lambda}, \quad 0 \le i \le N,\, 0 \le j \le P,$$
$$\boldsymbol{D}_{n,p} = d_{n,p}, \quad (\tilde{\boldsymbol{T}}_F)_{n,p} = \tilde{T}_{n,p}, \quad 0 \le n \le N,\, 0 \le p \le P.$$

For matrices $\boldsymbol{A} = (a_{i,j})$, $\boldsymbol{B} = (b_{i,j})$ we define the Hadamard product $\boldsymbol{A} * \boldsymbol{B} = (c_{i,j})$ with $c_{i,j} := a_{i,j} b_{i,j}$. Then the discrete problem (32) can be formulated as follows: determine $\boldsymbol{T}_F \in \mathbb{R}^{(N+1)\times(P+1)}$ such that

$$\boldsymbol{\mathcal{G}}(\boldsymbol{T}_F) := \boldsymbol{\mathcal{F}}^{-1}\big(\boldsymbol{D} * \boldsymbol{\mathcal{F}}(\boldsymbol{T}_F)\big) + \boldsymbol{M}(\boldsymbol{T}_F) * \boldsymbol{T}_F - \boldsymbol{G} = \boldsymbol{0}. \tag{33}$$

The above defines a nonlinear system in the (physical) unknown $\boldsymbol{T}_F$. Note the similarity to the continuous problem in (17)–(18). The equivalent representation in the (spectral) unknown $\tilde{\boldsymbol{T}}_F$ is given by

$$\boldsymbol{D} * \tilde{\boldsymbol{T}}_F + \boldsymbol{\mathcal{F}}\big(\boldsymbol{M}(\boldsymbol{\mathcal{F}}^{-1}(\tilde{\boldsymbol{T}}_F)) * \boldsymbol{\mathcal{F}}^{-1}(\tilde{\boldsymbol{T}}_F)\big) - \tilde{\boldsymbol{G}} = \boldsymbol{0}, \quad \text{with } \tilde{\boldsymbol{G}} := \boldsymbol{\mathcal{F}}(\boldsymbol{G}). \tag{34}$$

The nonlinearity of the problems (33) and (34) is contained in the terms $\boldsymbol{M}(\boldsymbol{T}_F) * \boldsymbol{T}_F$ and $\boldsymbol{\mathcal{F}}\big(\boldsymbol{M}(\boldsymbol{\mathcal{F}}^{-1}(\tilde{\boldsymbol{T}}_F)) * \boldsymbol{\mathcal{F}}^{-1}(\tilde{\boldsymbol{T}}_F)\big)$, respectively. The former has a much simpler structure and admits a more efficient numerical treatment. Therefore we used the physical representation (33) in our numerical simulations.

Remark 4 We claim that the important properties of the *continuous* operator $\mathcal{G}$ as formulated in Theorem 1 and Theorem 2 are inherited by the *discrete* operator $\boldsymbol{\mathcal{G}}$. To make this more precise we assume, for simplicity, $D_1 = 1$, $P = N$, which implies $\boldsymbol{V}_P = \boldsymbol{V}_N$. Let $N, k, \ell \in \mathbb{N}$ be such that $N \bmod k = 0$, $N \bmod \ell = 0$ and define $m_k := \frac{N}{k}$, $m_\ell := \frac{N}{\ell}$. Let $\boldsymbol{v}_r$ be the r-th column of $\boldsymbol{V}_N$. We introduce the following discrete analogon of the space $V_{k,\ell}$:

$$V_{k,\ell}^N := \operatorname{span}\big\{\, \boldsymbol{v}_{kn} \boldsymbol{v}_{\ell p}^T \mid 0 \le n \le m_k,\ 0 \le p \le m_\ell \,\big\}.$$

Note that $V_{k,\ell}^N$ is a $(m_k+1)\times(m_\ell+1)$-dimensional subspace of $\mathbb{R}^{(N+1)\times(N+1)}$. We claim that the following holds (cf. Theorem 1):

$$\boldsymbol{\mathcal{G}} :\, V_{k,\ell}^N \to V_{k,\ell}^N. \tag{35}$$

Furthermore, assume that $\boldsymbol{T} = \sum_{n=0}^{m_k} \sum_{p=0}^{m_\ell} \tilde{T}_{kn,\ell p} \boldsymbol{v}_{kn} \boldsymbol{v}_{\ell p}^T \in V_{k,\ell}^N$ satisfies $\boldsymbol{\mathcal{G}}(\boldsymbol{T}) = 0$. Define

$$\boldsymbol{T}^{*,1} = \sum_{n=0}^{m_k} \sum_{p=0}^{m_\ell} (-1)^n \tilde{T}_{kn,\ell p} \boldsymbol{v}_{kn} \boldsymbol{v}_{\ell p}^T, \quad \boldsymbol{T}^{*,2} = \sum_{n=0}^{m_k} \sum_{p=0}^{m_\ell} (-1)^p \tilde{T}_{kn,\ell p} \boldsymbol{v}_{kn} \boldsymbol{v}_{\ell p}^T,$$
$$\boldsymbol{T}^{*,3} = \sum_{n=0}^{m_k} \sum_{p=0}^{m_\ell} (-1)^{n+p} \tilde{T}_{kn,\ell p} \boldsymbol{v}_{kn} \boldsymbol{v}_{\ell p}^T.$$

We claim that

$$\boldsymbol{\mathcal{G}}(\boldsymbol{T}^{*,i}) = \boldsymbol{0} \quad \text{for } \ i = 1, 2, 3, \tag{36}$$

holds (cf. Theorem 2). Results as in (35)-(36) have been proven in [18] for the case of a 2D heater. In that case the fluid-heater interface is *one*-dimensional and thus (only) univariate

discrete Fourier analysis has been necessary to derive results as in (35)-(36) (theorems in [18], Section 3). Here we need a bivariate discrete Fourier analysis, which requires cumbersome technicalities that are beyond the present scope. For brevity we have chosen not to include these technical derivations in this paper and therefore present the results (35) and (36) as claims.

4.2 Continuation strategy

To determine solutions to the discrete nonlinear system (33) we employ a continuation method. The nonlinearity in the model is caused by the nonlinear boundary heat flux condition

$$q_F(T_F) = C_D \left\{F_1 - F_2 H(C_D T_F - 1)\right\} T_F$$

with coefficients C_D, F_1, F_2 and a Heaviside function $H(\cdot)$ as explained in Section 2.2. The model is linear if q_F is a linear function of T_F. This motivates our choice of the continuation parameter, denoted by λ: We define

$$q_F(T_F, \lambda) := C_D \left\{F_1 - \lambda F_2 H(C_D T_F - 1)\right\} T_F, \quad \text{for } \ 0 \le \lambda \le 1. \tag{37}$$

For $\lambda = 0$ we have a linear boundary condition; for $\lambda = 1$ the actual nonlinear condition is recovered. Figure 3 illustrates the smooth transition of the boiling curve $q_F(T_F, \lambda)$ from the linear state ($\lambda = 0$) to the final nonlinear state ($\lambda = 1$) in Figure 2*b*.

The discrete nonlinear problem (33) with the λ-dependent heat-transfer condition according to (37) can be represented as

$$\boldsymbol{\mathcal{G}}(\boldsymbol{T_F}, \lambda) := \boldsymbol{\mathcal{F}}^{-1}\big(\boldsymbol{D} * \boldsymbol{\mathcal{F}}(\boldsymbol{T}_F)\big) + \boldsymbol{M}_\lambda(\boldsymbol{T}_F) * \boldsymbol{T}_F - \boldsymbol{G} = \boldsymbol{0}. \tag{38}$$

Note that $\boldsymbol{M}_\lambda(\boldsymbol{T}_F)$ depends on λ via $\big(\boldsymbol{M}_\lambda(\boldsymbol{T}_F)\big)_{i,j} = \alpha_\lambda(T_F(x_i, y_j))$ for $0 \le i \le N, 0 \le j \le P$ with $\alpha_\lambda(T_F) = \frac{\Pi_2}{\Lambda}\frac{q_F(T_F,\lambda)}{T_F}$ and $q_F(T_F, \lambda)$ as in (37). For each $\lambda \in [0, 1]$ the set of *homogeneous* solutions (i.e. $\boldsymbol{T}_F$ =constant) of this system can be easily computed. Starting on a branch of homogeneous solutions we apply a continuation algorithm[2] to $\lambda \to \boldsymbol{\mathcal{G}}(\boldsymbol{T}_F, \lambda) = \boldsymbol{0}$ and determine bifurcations points on the homogeneous branches from which branches of heterogeneous solutions originate. This strategy is used in the numerical simulations in the next section.

5 Numerical experiments: a representative case study

In this section we consider the discrete steady-state problem for a fixed parameter set, namely $\Lambda = 0.2$, $D_1 = 1$ (square interface), $D_2 = 0.2$, $\Pi_1 = 4$, $\Pi_2 = 2$ and $W = 1$. The set of steady-state solutions is determined with the approach introduced in Section 4. Homogeneous solutions are obtained by means of a standard Newton-type root-finding algorithm applied to (12); heterogeneous solutions follow from continuation of the nonlinear system (38) in the nonlinearity parameter λ. Important to note is that for smooth boiling curves (i.e. $W > 0$) the truncated Fourier expansion that underlies (38) exhibits exponential convergence. Hence,

[2]Here an in-house algorithm of the Chair of Process Systems Engineering, RWTH Aachen, has been used that is based upon techniques described in [9]. Elaboration on this continuation algorithm is beyond the scope of this paper.

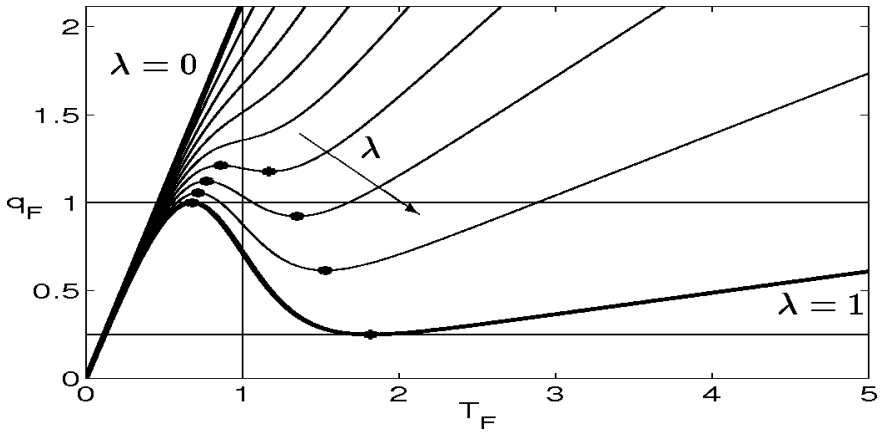

Figure 3: *Controlling the degree of nonlinearity of the boiling curve via the nonlinearity parameter λ. Shown is the smooth transition from a linear profile ($\lambda = 0$) towards the physical boiling curve (heavy; $\lambda = 1$) with increasing λ (arrow). The stars are the local maximum and minimum that occur for λ beyond some non-zero lower limit.*

the continuation algorithm yields highly-accurate approximations to the continuous solution at any position $(x, y) \in \Gamma_F$ for moderate values of N and P. Here $(N, P) = (36, 36)$ has been used.

5.1 Homogeneous solutions

The homogeneous steady-state solutions (13) correspond to the constant interface temperature $T_F = \widetilde{T}_{0,0}$ determined by (12). This interface temperature is given by the (multiple) intersection(s) of the boiling curve with the normalised heat-supply $\bar{q}_H/Q_C = \Pi_2^{-1}$ (Figure 2*b*). To determine the physically-meaningful homogeneous solutions it is sufficient to resolve (12) for $\lambda = 1$. However, for the continuation strategy, in which heterogeneous solution branches originate from homogeneous branches, we need the homogeneous branches in the entire range $0 \leq \lambda \leq 1$. These branches readily follow from solving (12) in this λ-range. Two essentially different situations occur, as illustrated in Figure 4, namely: (i) one solution $T_F^{(1)}$ for $0 \leq \lambda < \lambda_*$ (Figure 4*a*); (ii) three solutions $(T_F^{(1)}, T_F^{(2)}, T_F^{(3)})$ for $\lambda_* < \lambda \leq 1$ (Figure 4*c*). Both situations are connected through the degenerate case $\lambda = \lambda_*$, for which the local minimum of the boiling curve q_F is tangent to the normalised heat supply $\bar{q}_H/Q_C = \Pi_2^{-1}$, causing the second and third solutions to coincide (Figure 4*b*). Thus the system undergoes a qualitative change at $\lambda = \lambda_*$ through a so-called tangent bifurcation [15].

The homogeneous solutions as a function of the nonlinearity parameter λ are shown in the bifurcation diagram in Figure 5. Solutions are represented in terms of the functional $T_\Sigma = \sum_{n,p} \widetilde{T}_{n,p}$. The lower (nearly-horizontal) branch corresponds to the intersection $T_F^{(1)}$ that exists for all $0 \leq \lambda \leq 1$; the upper branch, with turning point at λ_* (dot), coincides with the two intersections $T_F^{(2,3)}$ that exist only in the interval $\lambda_* \leq \lambda \leq 1$ (here $\lambda_* \approx 0.926$). The lower and upper legs of this upper branch (connecting at the turning point at $\lambda = \lambda_*$) correspond with $T_F^{(2)}$ and $T_F^{(3)}$, respectively.

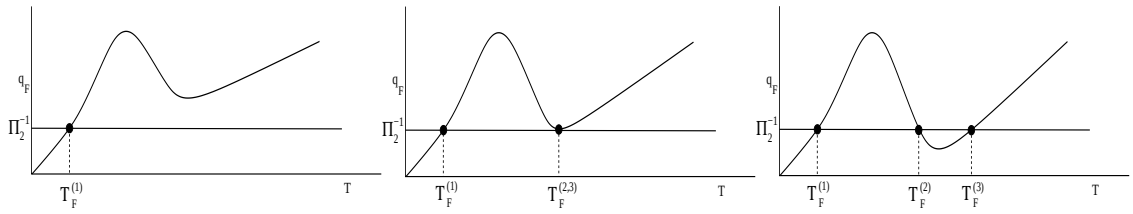

a) $\lambda < \lambda_*$ *b)* $\lambda = \lambda_*$ *c)* $\lambda > \lambda_*$

Figure 4: *Homogeneous solutions of the nonlinear system as a function of the nonlinearity parameter* λ*. Transition from the single-solution state (panel a) to the triple-solution state (panel c) takes place via the tangent bifurcation at* $\lambda = \lambda_*$ *(panel b).*

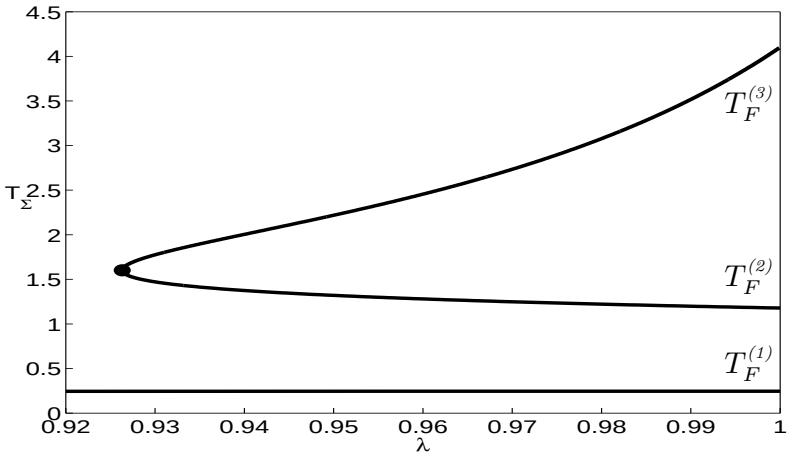

Figure 5: *Bifurcation diagram for the homogeneous solutions associated with the nonlinearity parameter* λ*. The lower branch is the intersection* $T_F^{(1)}$ *that exists for all* $0 \le \lambda \le 1$*; the upper branch, with turning point at* λ_* *(dot), coincides with the two intersections* $T_F^{(2,3)}$ *that exist only in the interval* $\lambda_* \le \lambda \le 1$ *(here* $\lambda_* \approx 0.926$*). The lower and upper legs of this upper branch (connecting at the turning point at* $\lambda = \lambda_*$*; dot) correspond with* $T_F^{(2)}$ *and* $T_F^{(3)}$*, respectively.*

5.2 Bifurcation points on branches of homogeneous solutions

Multiple (heterogeneous) solutions emerge through bifurcations of the function $\lambda \to \boldsymbol{T}_F(\lambda)$, where $\boldsymbol{T}_F(\lambda)$ is a homogeneous solution of $\boldsymbol{\mathcal{G}}(\boldsymbol{T}_F, \lambda) = \boldsymbol{0}$. Bifurcations occur at λ-values for which the Jacobian of $\boldsymbol{\mathcal{G}}$ with respect to $\boldsymbol{T}_F$ is singular [9]. This Jacobian is given by

$$\boldsymbol{J} = \frac{\partial \boldsymbol{\mathcal{G}}(\boldsymbol{T}_F, \lambda)}{\partial \boldsymbol{T}_F}, \quad \boldsymbol{J}: \ \boldsymbol{W} \to \boldsymbol{\mathcal{F}}^{-1}\big(\boldsymbol{D} * \boldsymbol{\mathcal{F}}(\boldsymbol{W})\big) + \boldsymbol{Q}(\boldsymbol{T}_F, \lambda) * \boldsymbol{W}, \tag{39}$$

with

$$(\boldsymbol{Q}(\boldsymbol{T}_F, \lambda))_{i,j} \ = \gamma((T_F)_{i,j}, \lambda) \quad 0 \le i \le N,\, 0 \le j \le P, \quad \gamma(T_F, \lambda) \ := \frac{\Pi_2}{\Lambda} \frac{\partial q_F(T_F, \lambda)}{\partial T_F}.$$

On a homogeneous branch we have $\boldsymbol{T}_F = T_F\mathbf{1}$, with

$$\mathbf{1} = \begin{pmatrix} 1 & \dots & 1 \\ \vdots & & \vdots \\ 1 & \dots & 1 \end{pmatrix} \in \mathbb{R}^{(N+1)\times(P+1)},$$

and T_F the homogeneous interface temperature. This implies $\boldsymbol{Q}(\boldsymbol{T}_F, \lambda) = \gamma(T_F, \lambda)\mathbf{1}$ and thus on a homogeneous branch the Jacobian simplifies to

$$\boldsymbol{J}\big(\boldsymbol{W}\big) = \boldsymbol{\mathcal{F}}^{-1}\big(\boldsymbol{D} * \boldsymbol{\mathcal{F}}(\boldsymbol{W})\big) + \gamma(T_F, \lambda)\boldsymbol{W} = \boldsymbol{\mathcal{F}}^{-1}\left\{(\boldsymbol{D} + \gamma(T_F, \lambda)\mathbf{1}) * \boldsymbol{\mathcal{F}}(\boldsymbol{W})\right\}. \tag{40}$$

The Jacobian $\boldsymbol{J}$ is singular iff there exists a $\boldsymbol{W} \neq \mathbf{0}$ such that $\boldsymbol{J}(\boldsymbol{W}) = \mathbf{0}$. For the Jacobian in (40) this is equivalent to

$$(\boldsymbol{D} + \gamma(T_F, \lambda)\mathbf{1}) * \widetilde{\boldsymbol{W}} = \mathbf{0}, \tag{41}$$

for a $\widetilde{\boldsymbol{W}} \neq \mathbf{0}$, with $\widetilde{\boldsymbol{W}} = \boldsymbol{\mathcal{F}}(\boldsymbol{W})$, which, in turn, is equivalent to

$$\zeta_{n,p}\widetilde{W}_{n,p} = 0 \quad \forall n, p, \qquad \zeta_{n,p} := d_{n,p} + \gamma(T_F, \lambda), \tag{42}$$

with $\widetilde{W}_{n,p}$ the spectrum of $\boldsymbol{W}$ and $d_{n,p}$ as in (16). Non-zero $\widetilde{\boldsymbol{W}}$ requires $\widetilde{W}_{n,p} \neq 0$ and $\zeta_{n,p} = 0$ for at least one wave-number pair (n, p). This implies that non-trivial solutions $\boldsymbol{W}$ of $\boldsymbol{J}(\boldsymbol{W}) = \mathbf{0}$ are of the form

$$\boldsymbol{W} = \sum_{i=1}^{m} \widetilde{W}_{n_i,p_i}\boldsymbol{v}_{N,n_i}\boldsymbol{v}_{P,p_i}^T, \quad \text{with } (n_i, p_i) \text{ such that } \zeta_{n_i,p_i} = 0,\ 1 \leq i \leq m. \tag{43}$$

Here $\boldsymbol{v}_{N,r}$ ($\boldsymbol{v}_{P,r}$) denotes the r-th column of the matrix $\boldsymbol{V}_N$ ($\boldsymbol{V}_P$) and m is the number of vanishing coefficients $\zeta_{n,p}$, $0 \leq n \leq N, 0 \leq p \leq P$. Null solutions (43) are linear combinations of the m Fourier modes $\boldsymbol{v}_{N,n}\boldsymbol{v}_{P,p}^T$ that correspond with vanishing coefficients $\zeta_{n,p}$; the associated bifurcation (point) is called an "m-mode bifurcation". The expansion coefficients $\widetilde{W}_{n_i,p_i}$ are free, implying that null solutions span an m-dimensional nullspace with as basis vectors the Fourier modes in (43). Because $d_{n,p} \geq 0$ for all $n, p \geq 0$, vanishing coefficients $\zeta_{n,p}$ require $\gamma(T_F, \lambda) < 0$ and thus a bifurcation on a homogeneous solution branch can only occur for those T_F for which the boiling curve has a negative slope ($\dot{q}_F \leq 0$). From Figure 4 it follows that only intersection $T_F^{(2)}$ meets this criterion, which implies that bifurcations are restricted to the $T_F^{(2)}$-branch in the bifurcation diagram (Figure 5). This results in the fundamental property that *bifurcations – and thus multiple (heterogeneous) solutions – are essentially a transition phenomenon.* Figure 6*a* displays γ (heavy curve) as a function of λ on the $T_F^{(2)}$-branch together with $-d_{n,p}$ (dashed lines) for $p = 0$ and various n.

The intersections $\gamma = -d_{n,p}$ correspond to $\zeta_{n,p} = 0$ and thus define the λ-values at which the system undergoes a bifurcation. Figure 6*a* reveals that $\zeta_{n,p} = 0$ occurs for the case $p = 0$ only for $n = 0, 1, 2, 3$. Furthermore, the monotonic decay of γ with increasing λ causes the intersections – and corresponding bifurcations – to occur in successive order $n = 0, 1, 2, 3$ from left to right. With a similar monotonicity argument it follows that the number of intersections decreases monotonically with increasing p. This implies that vanishing coefficients $\zeta_{n,p}$ correspond with those wave numbers $0 \leq n \leq n_{max}(p)$ that satisfy the inequality $d_{n,p} + \gamma_{min} \leq 0$, with $\gamma_{min} = \gamma(T_F)|_{\lambda=1}$. Figure 6*b* gives $-d_{n,p}$ (circles) for $0 \leq n \leq 3$ as a function of the wave number p; wave number n increases top down (arrow). The crosses mark the values $-d_{n,p}$

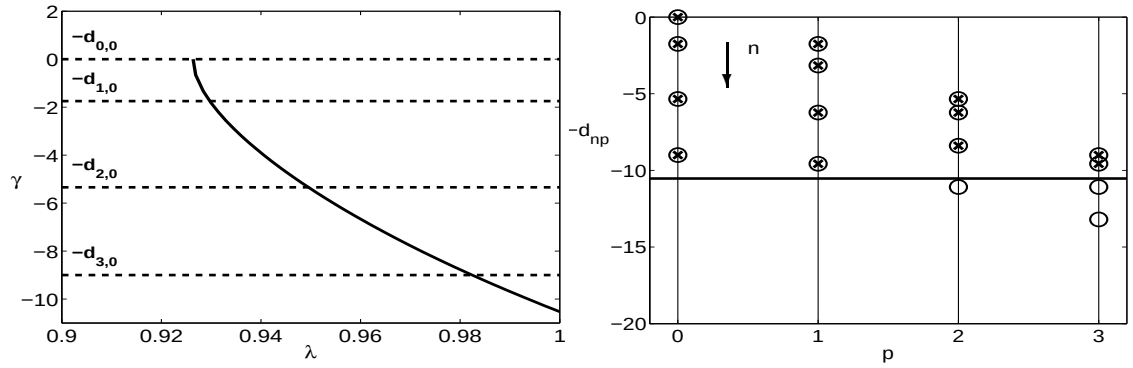

a) *b)*

Figure 6: *Occurrence of bifurcations on the homogeneous $T_F^{(2)}$-branch. Panel a shows function $\lambda \to \gamma(T_F(\lambda)) = \Pi_2 \dot{q}_F(T_F(\lambda))/\Lambda$ along the $T_F^{(2)}$-branch (heavy). The dashed horizontal lines are the values of $-d_{n,p}$. Intersections of γ with $-d_{n,p}$ correspond to a singular Jacobian $\boldsymbol{J}$ and thus to a bifurcation. Panel b shows $-d_{n,p}$ (circles) for $0 \leq n \leq 3$ as a function of the wave number p. Wave number n increases top down (arrow). The crosses mark the values $-d_{n,p}$ above $\gamma_{min} = \gamma(T_F)|_{\lambda=1}$ (heavy) and highlight those wave-number pairs (n, p) for which the system undergoes a bifurcation.*

above γ_{min} (heavy) and thus highlight those wave-number pairs (n, p) for which $\zeta_{n,p} = 0$ for some $\lambda \in [0, 1]$ and the system undergoes a bifurcation. It readily follows that here $0 \leq p \leq 3$ and $n_{max}(p) = 3, 3, 2, 1$ for $p = 0, 1, 2, 3$.

Figure 7*a* gives the wave-number pairs (k, ℓ) (stars) for which the present configuration undergoes a bifurcation (Figure 6*b*). The symmetric arrangement of these wave-number pairs w.r.t. the diagonal $k = \ell$ is a manifestation of the square interface (Lemma 1): pairs on the diagonal $k = \ell$ correspond with one single vanishing coefficient $\zeta_{k,\ell} = 0$ (1-mode bifurcation); pairs off the diagonal $k = \ell$ form couples of wave-number pairs ("wave-number groups") $[(k, \ell), (\ell, k)]$ that correspond with two vanishing coefficients $\zeta_{k,\ell} = \zeta_{l,k} = 0$ (2-mode bifurcation). The 1-mode and 2-mode bifurcations are indicated by dots and stars, respectively, in Figure 7*b*. The resulting heterogeneous solutions are discussed below.

5.3 Heterogeneous solutions

In this section we study the (multiple) heterogeneous solutions that occur in our case study (recall that we consider a square heater). From the analysis above it follows that heterogeneous solutions emerge from bifurcations on the homogeneous $T_F^{(2)}$-branch. The first bifurcation (turning point) on the $T_F^{(2)}$-branch corresponds with one single vanishing coefficient $\zeta_{k,\ell}$ for $k = l = 0$ and thus, due to (43), the nontrivial solution $\boldsymbol{W}$ corresponds to a zero-th Fourier-mode, i.e., a constant. The solution that emerges from this bifurcation point is homogeneous. Thus the first bifurcation point is of tangent type (Figure 4*b*) that results in two additional homogeneous solutions. The remaining bifurcations have at least one non-zero wave number and thus involve heterogeneous bifurcation solutions. Two types of such bifurcation points occur in the current configuration: 1-mode and 2-mode bifurcations. The former occur for $k = \ell$ (dots in Figure 7*b*) and the latter for $k \neq \ell$ (stars in Figure 7*b*). Below we treat these two types separately.

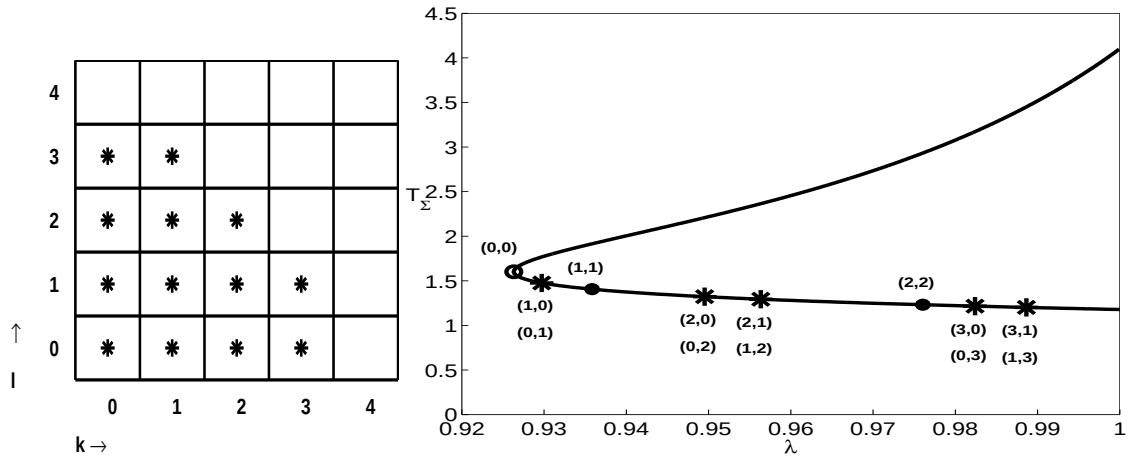

a) *b)*

Figure 7: *Bifurcation points in the case study:* $\Lambda = 0.2$, $D_1 = 1$, $D_2 = 0.2$, $\Pi_1 = 4$, $\Pi_2 = 2$ *and* $W = 1$. *Panel a gives the wave-number pairs* (k, ℓ) *(stars) for which the present configuration undergoes a bifurcation (Figure 6b). Bifurcations on the diagonal* $k = \ell$ *correspond to one single vanishing coefficient* $\zeta_{k,k} = 0$ *(1-mode bifurcation); pairs off the diagonal* $k = \ell$ *form wave-number groups* $[(k, \ell), (\ell, k)]$, $k \neq \ell$, *that correspond with two vanishing coefficients* $\zeta_{k,\ell} = \zeta_{\ell,k} = 0$ *(2-mode bifurcation). Panel b gives the bifurcations on the homogeneous* $T_F^{(2)}$*-branch with corresponding wave numbers* (k, ℓ) *as indicated.*

1-mode bifurcations

For 1-mode bifurcations the null solutions (43) reduce to individual Fourier modes ($m = 1$) and, consequently, heterogeneous solutions of the form

$$T_F(x, y) = T_F^{(2)} + \epsilon \cos(k\pi x) \cos(k\pi y), \qquad \epsilon \downarrow 0, \tag{44}$$

emerge ("1-mode bifurcation solution"). This function is an element of the Fourier space $V_{k,k}$. Based on Theorem 1 we conclude that solution branches emerging from the 1-mode bifurcation remain in the Fourier space $V_{k,k}$ (provided no further bifurcation occurs). The bifurcation solution (44) is of the generic form (19) with $\widetilde{T}_{kn,kp} \neq 0$ for $n = p = 1$ and $\widetilde{T}_{kn,kp} = 0$ otherwise. From Theorem 2 it follows that there are corresponding shifted dual solutions with the self-symmetry properties $T_F(x, y) = T_F^{*,3}(x, y)$, $T_F^* := T_F^{*,1}(x, y) = T_F^{*,2}(x, y)$ and $T_F^* \neq T_F$. Moreover, Lemma 1 implies that in the present case of a square heater each solution has a dual reflected solution. However, one easily verifies that, since (44) implies $T_F(x, y) = T_F(y, x)$, these dual reflected solutions coincide with the original ones: $T_F = T_F'$ and $T_F^{*\prime} = T_F^*$. Thus we conclude that there is a pitchfork bifurcation with a *pair* (T_F, T_F^*) of solutions emerging from the 1-mode bifurcations in Figure 7*b* (dots). Due to Theorem 1 (cf. also Remark 3) *these symmetry properties are preserved along the solution branches.* Figure 8 shows the solutions for $k = 2$ emerging from the bifurcations (panels *a* and *b*) and the corresponding final states at $\lambda = 1$ (panels *c* and *d*). Figure 12 (first column) shows the final states ($\lambda = 1$) of the pairs of solutions corresponding with the 1-mode bifurcations, both for $k = 1$ and $k = 2$.

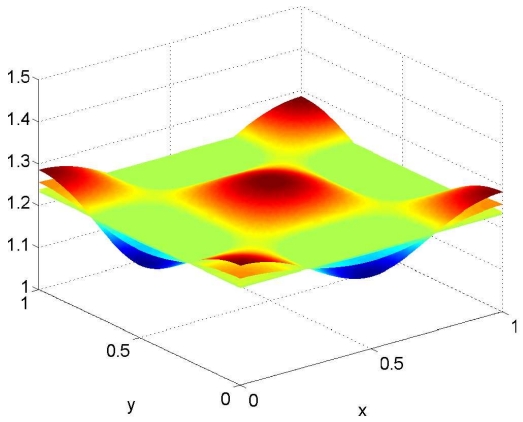

a) T_F: proximity of bifurcation ($\lambda \approx 0.976$).

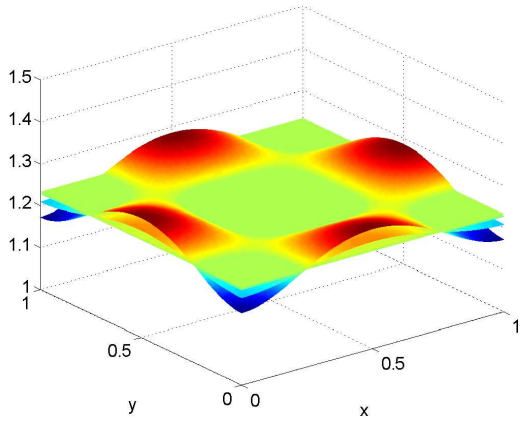

b) T_F^*: proximity of bifurcation ($\lambda \approx 0.976$).

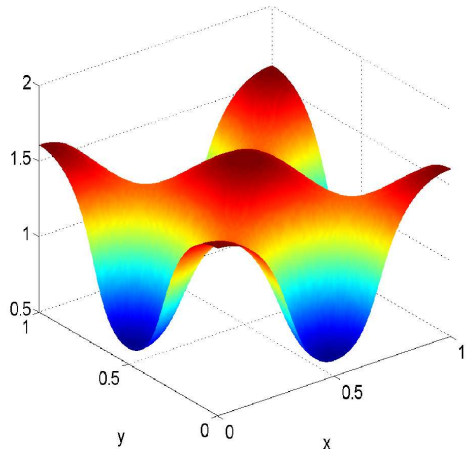

c) T_F: final state ($\lambda = 1$).

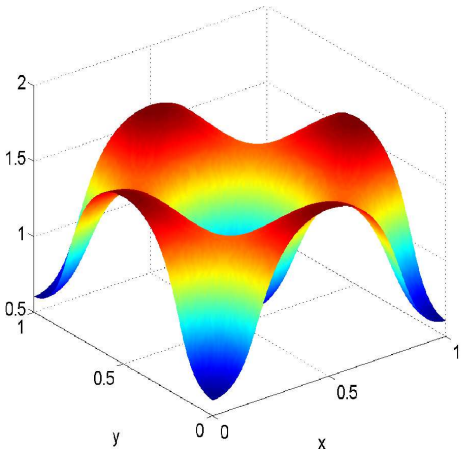

d) T_F^*: final state ($\lambda = 1$).

Figure 8: *Pairwise emergence of heterogeneous solutions from 1-mode bifurcations for the case $k = 2$. Panels a and b show T_F and its dual shifted solution T_F^*, for a $\lambda-$value close to the bifurcation point ($\lambda = 0.97605$); panels c and d show the corresponding final states ($\lambda = 1$) of T_F and its dual shifted solution T_F^*. The final states are the physically-meaningful steady-state solutions to the boiling problem.*

2-mode bifurcations

For 2-mode bifurcations the null solutions (43) are spanned by two Fourier modes ($m = 2$) with wave numbers (k, ℓ) and (ℓ, k), $\ell \neq k$ (due to $\zeta_{k,\ell} = \zeta_{\ell,k} = 0$) and yield

$$T_F(x, y) = T_F^{(2)} + \epsilon\big(c_1 \cos(k\pi x)\cos(l\pi y) + c_2 \cos(l\pi x)\cos(k\pi y)\big), \qquad \epsilon \downarrow 0, \tag{45}$$

as associated 2-mode bifurcation solution. Such 2-mode bifurcation solutions (45) involve a two-dimensional nullspace spanned by the two associated Fourier modes. This is a fundamental difference with the 2D pool-boiling problem, which admitted only simple vanishing coefficients $\zeta_{k,\ell}$ and thus only one-dimensional nullspaces [18]. The occurrence of higher (than one) dimensional null spaces appears to be an essentially 3D phenomenon.

Multi-dimensional null spaces imply infinite families of bifurcation solutions (45) and thus in principle an infinite family of corresponding branching solutions might occur. However,

extensive numerical experiments strongly suggest that (only) the following four classes of 2-mode solutions exist:

$$c_1 \neq 0,\ c_2 = 0 \quad (\text{“quasi 1-mode”}), \tag{46}$$
$$c_1 = 0,\ c_2 \neq 0 \quad (\text{“quasi 1-mode”}), \tag{47}$$
$$c_1 = c_2 \neq 0 \quad (\text{“true 2-mode”}), \tag{48}$$
$$c_1 = -c_2 \neq 0 \quad (\text{“true 2-mode”}). \tag{49}$$

The first two classes correspond to 1-mode simplifications of (45) whereas the other two classes correspond to truly 2-mode bifurcation solutions. A theoretical explanation for the fact that (only) these classes of solutions occur is not available yet.
Each of these four classes consists of multiple solutions. To explain the structure of this multiplicity we treat the first and third classes in more detail. The second and fourth classes have properties very similar to the first and third classes, respectively.

Case $\mathbf{c_1 \neq 0},\ \mathbf{c_2 = 0}$
In this case the bifurcation solutions (45) reduce to individual Fourier modes and heterogeneous solutions of the form

$$T_F(x,y) = T_F^{(2)} + \epsilon \cos(k\pi x)\cos(\ell\pi y), \qquad \epsilon \downarrow 0, \quad k \neq \ell, \tag{50}$$

with $0 \leq k, \ell \leq 3,\ k + \ell \leq 4$, cf. Fig. 7, emerge (“quasi 1-mode bifurcation solution”). The function in (50) is an element of the Fourier space $V_{k,\ell}$. Based on Theorem 1 we conclude that solution branches emerging from such a bifurcation remain in the Fourier space $V_{k,\ell}$ (provided no further bifurcation occurs). We first consider pairs (k,ℓ) with $k \neq 0$ and $\ell \neq 0$. The bifurcation solution (50) is of the generic form (19) with $\widetilde{T}_{0,0} = T_F^{(2)}$, $\widetilde{T}_{kn,\ell p} = \epsilon$ for $n = p = 1$ and $\widetilde{T}_{kn,\ell p} = 0$ otherwise. From Theorem 2 it follows that there are corresponding shifted dual solutions with the self-symmetry properties $T_F(x,y) = T_F^{*,3}(x,y)$, $T_F^* := T_F^{*,1}(x,y) = T_F^{*,2}(x,y)$ and $T_F^* \neq T_F$. Lemma 1 yields that each of these two solutions has a reflected solution. One easily checks that, as opposed to the case $k = \ell$ considered above, these reflected solutions differ from T_F and T_F^*. Thus we obtain the following cluster of *four* different solutions:

$$T_F \text{ as in (50)}, \quad T_F^* := T_F^{*,1} = T_F^{*,2}, \quad T_F', T_F^{*\prime} \text{ as in Lemma 1.} \tag{51}$$

The symmetry properties are preserved along the solution branches. Thus we conclude that for $\lambda = 1$ we have a cluster of 4 solutions with the same symmetry properties as in (51). Note that for $T_F = T_F|_{(k,\ell)}$ as in (50) we have $T_F|_{(k,\ell)} = T_F'|_{(\ell,k)}$. From this one easily deduces that the clusters (51) for (k,ℓ) and (ℓ,k) are the same. In Figure 12 these clusters are shown for $(k,\ell) = (2,1)$ (second column) and for $(k,\ell) = (3,1)$ (third column). As noted above, for $(k,\ell) = (1,2)$ and $(k,\ell) = (1,3)$ the clusters are the same as in column 2 and 3, respectively.

We now consider $\ell = 0,\ k \in \{1,2,3\}$. Note that in this case the Fourier mode in (50) is constant in y-direction (“semi-heterogeneous solution”). From Theorem 2 (with $\ell = \infty$) it follows that there are corresponding shifted dual solutions with the self-symmetry properties $T_F(x,y) = T_F^{*,2}(x,y)$, $T_F^* := T_F^{*,1}(x,y) = T_F^{*,3}(x,y)$ and $T_F^* \neq T_F$. Lemma 1 yields that each of these two solutions has a reflected solution. These reflected solutions differ from T_F and T_F^*. Thus we again obtain a cluster of *four* different solutions:

$$T_F \text{ as in (50)}, \quad T_F^* := T_F^{*,1} = T_F^{*,3}, \quad T_F', T_F^{*\prime} \text{ as in Lemma 1.} \tag{52}$$

The same holds (with $T_F^{*,1}$ and $T_F^{*,2}$ interchanged) for the case $k = 0,\ \ell \in \{1, 2, 3\}$. The semi-heterogeneous solutions for the case $\ell = 0$ are illustrated in Figure 9

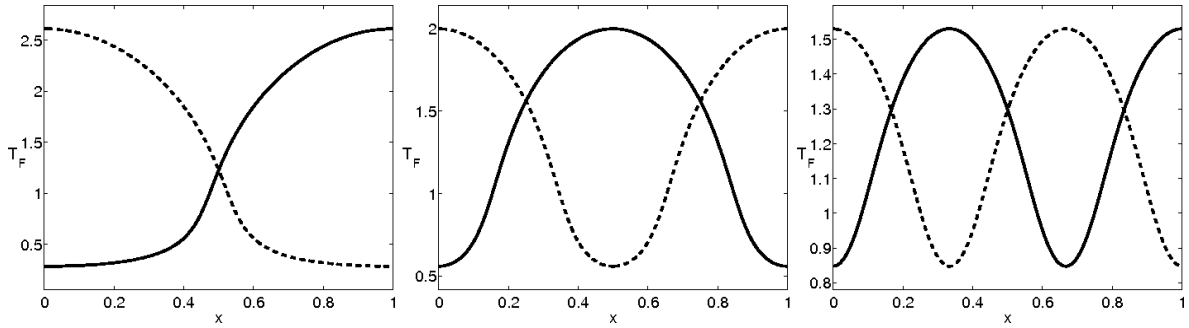

a) (T_F, T_F^*) *for* $(k, \ell) = (1, 0)$. *b)* (T_F, T_F^*) *for* $(k, \ell) = (2, 0)$. *c)* (T_F, T_F^*) *for* $(k, \ell) = (3, 0)$.

Figure 9: *Physically-meaningful* ($\lambda = 1$) *semi-heterogeneous solutions emerging from the quasi 1-mode bifurcation solution. Shown are cross-sections (y fixed) of the temperature profiles* T_F *(solid) and* T_F^* *(dashed) for wave-numbers* $\ell = 0,\ k = 1, 2, 3$. *The profiles of* T_F' *and* $T_F^{*\prime}$ *are obtained by interchanging* x *and* y.

We conclude that for the case (46) a class of four different heterogeneous solutions as in (51) or (52) exists. Using symmetry arguments one can show that in case (47), $c_1 = 0$ and $c_2 \neq 0$, *the same* clusters of four solutions as in (51) (for $k \neq 0, \ell \neq 0$), (52) (for $k = 0$) occur.

Case $\mathbf{c_1 = c_2 \neq 0}$

In this case the bifurcation solutions (45) are of the form

$$T_F(x, y) = T_F^{(2)} + \epsilon\big(\cos(k\pi x)\cos(\ell\pi y) + \cos(\ell\pi x)\cos(k\pi y)\big), \quad \epsilon \downarrow 0, \quad k \neq \ell, \tag{53}$$

("true 2-mode solution"). Let $q \in \mathbb{N}$ be the maximal common divisor of k and ℓ, i.e., $q \in \mathbb{N}$ is the maximal number such that $k_q := \frac{k}{q} \in \mathbb{N}$ and $\ell_q := \frac{\ell}{q} \in \mathbb{N}$. Note that if $\ell = 0$ ($k = 0$) then we have $q = k$ ($q = \ell$) and that if $k\ell \neq 0$ then *not* both k_q and ℓ_q can be even. We first consider the case $\ell = 0$, $k > 0$. Then T_F in (53) is of the form

$$T_F(x, y) = T_F^{(2)} + \epsilon\big(\cos(k\pi x) + \cos(k\pi y)\big). \tag{54}$$

This function is an element of the Fourier space $V_{k,k}$ and has the generic form (19) with

$$\widetilde{T}_{0,0} = T_F^{(2)}, \quad \widetilde{T}_{k,0} = \widetilde{T}_{0,k} = \epsilon \quad \text{and} \quad \widetilde{T}_{kn,kp} = 0 \ \text{ otherwise.} \tag{55}$$

From Theorem 2 it follows that there are shifted dual solutions $T_F^{*,i}$, $i = 1, 2, 3$. Using (23) and (55) it follows that these dual solutions are different from each other and from T_F. For the reflected dual solutions we have $T_F' = T_F$, $(T_F^{*,1})' = T_F^{*,2}$, $(T_F^{*,2})' = T_F^{*,1}$, $(T_F^{*,3})' = T_F^{*,3}$ and thus these reflections do not yield new solutions. Hence, for $k > 0$, $\ell = 0$ we obtain a cluster of *four* different solutions:

$$T_F \quad \text{as in (54)}, \quad T_F^{*,i},\ i = 1, 2, 3. \tag{56}$$

Again, these symmetry properties are preserved during the continuation. For $\lambda = 1$ the cluster of four solutions is shown in Figure 13.

The case $k = 0$, $\ell > 0$ leads to similar results (interchange x and y). The cluster of solutions for $(0, \ell)$ is the same as for $(\ell, 0)$.

For $k > 0$, $\ell > 0$ we have a bifurcating solution of the form

$$T_F(x, y) = T_F^{(2)} + \epsilon\big(\cos(k_q q\pi x)\cos(\ell_q q\pi y) + \cos(\ell_q q\pi x)\cos(k_q q\pi y)\big).$$

This function is an element of the Fourier space $V_{q,q}$. Using Theorem 2, Lemma 1 and symmetry arguments one can show that we have the following multiple solutions:

$$\text{a cluster of four solutions } \; T_F,\, T_F^{*,i},\; i = 1, 2, 3, \quad \text{if } \; k_q + \ell_q \; \text{ is odd,} \tag{57}$$

$$\text{a cluster of two solutions } \; T_F = T_F^{*,3},\, T_F^* := T_F^{*,1} = T_F^{*,2} \quad \text{if } \; k_q + \ell_q \; \text{ is even.} \tag{58}$$

(Recall that not both k_q and ℓ_q can be even). Thus we conclude that for the case $c_1 = c_2 \neq 0$ the clusters of solutions that occur are given in (56), (57), (58).

For the case (49), $c_1 = -c_2 \neq 0$, a similar analysis can be performed. It turns out that for $k > 0$, $\ell = 0$ the same cluster of four solutions as in (56) occurs. For $k > 0$, $\ell > 0$ and $k_q + \ell_q$ odd we get the same cluster of four solutions as in (57). For $k_q + \ell_q$ even we obtain a cluster of two solutions that are *different* from the two solutions in (58).

We summarise the results on heterogeneous solutions derived in this section. First note that in our case study we have $k_q + l_q$ even (cf. (58)) only for $(k, \ell) = (\ell, k) = (1, 3)$. The following clusters of solutions occur:

- Wave numbers (k, k), $k = 0, 1, 2$; There is a cluster of two 1-mode bifurcation solutions.
- Wave numbers (k, ℓ), $k \neq \ell$; There is a cluster of four quasi 1-mode bifurcation solutions ($c_1 = 0$ or $c_2 = 0$). If $k = 0$ or $\ell = 0$ there is a cluster of four true 2-mode bifurcation solutions. For $k\ell > 0$ we distinguish $k_q + \ell_q$ odd and $k_q + \ell_q$ even. In the former case there is a cluster of four true 2-mode bifurcation solutions. In the latter case we have two clusters each consisting of two true 2-mode bifurcation solutions.
  The full set of (different) solutions for wave number (k, ℓ) is identical to the set of all solutions for wave number (ℓ, k).

Thus for $(k, \ell) = (1, 2)$ we have a cluster of four true 2-mode solutions and for $(k, \ell) = (1, 3)$ we have two clusters with each two true 2-mode solutions. Figure 10 shows one solution ("parent") T_F from each of these clusters.

Figure 11 gives the bifurcation diagram including the full set of solutions found for the case study. For each *cluster* we show only the branch for *one parent solution* (T_F) from that cluster. Note that only for $(k, \ell) = (1, 3)$ we have *two* clusters of true 2-mode solutions and therefore two dashed branches in figure 11. For $\lambda = 1$ there is a total number of 44 different heterogeneous solutions.

We conclude this section on the case study with the following remark:

Remark 5 A preliminary stability analysis through numerical simulation of the unsteady problem (4) shows that all heterogeneous solutions as well as the homogeneous solution $T_F^{(2)}$ are unstable in time. Only the homogeneous solutions in the nucleate ($T_F^{(1)}$) and film ($T_F^{(3)}$) boiling regimes appear to be stable. Other solutions converge (for $t \to \infty$) to one of the two stable solutions. However, heterogeneous solutions involving "large" length scales (small wave numbers) can survive for relatively long times. A stability analysis will be presented in a forthcoming paper.

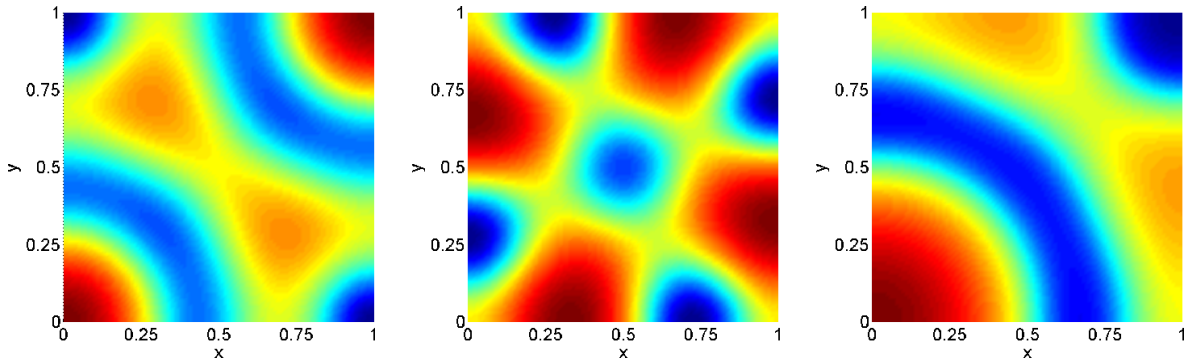

a) $(k,\ell) = (1,3)$*, cluster 1.* *b)* $(k,\ell) = (1,3)$*, cluster 2.* *c)* $(k,\ell) = (1,2)$.

Figure 10: *Physically-meaningful* ($\lambda = 1$) *heterogeneous (parent) solutions from 2-mode bifurcation solution clusters. Panels a and b: (parent) solutions of the two true 2-mode clusters for* $(k,\ell) = (1,3)$*. Panel c: (parent) solution of the cluster for* $(k,\ell) = (1,2)$.

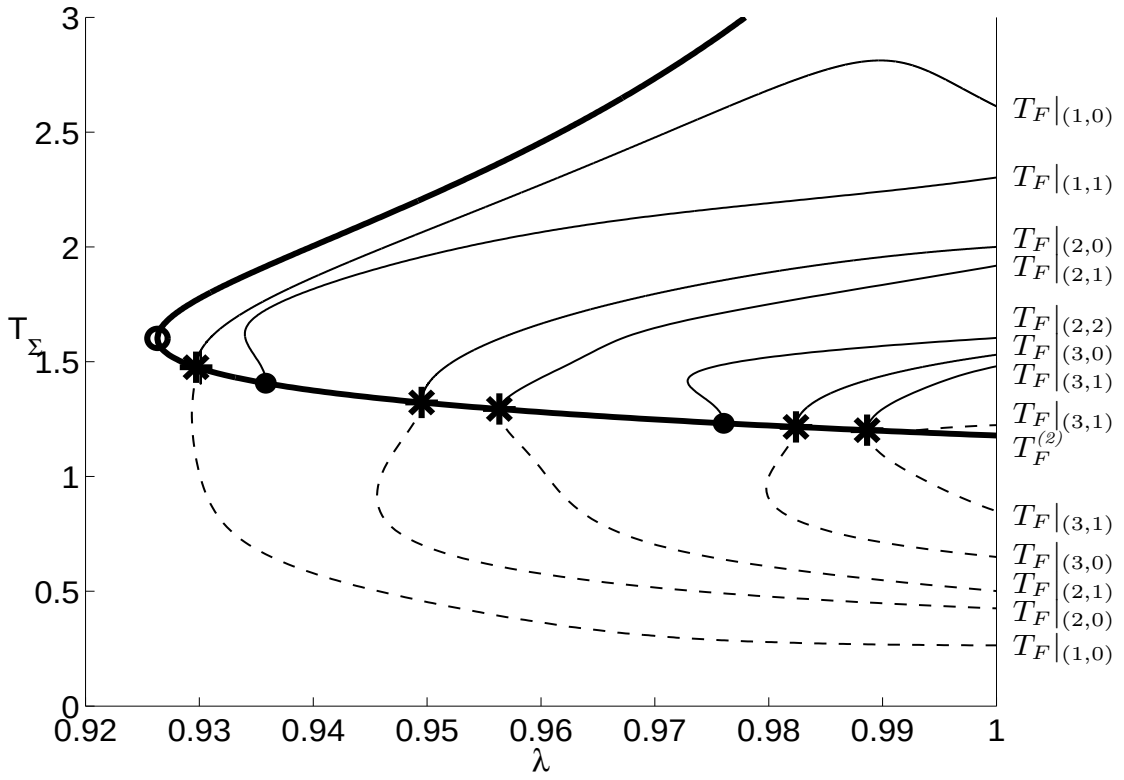

Figure 11: *Bifurcation diagram. Shown are the homogeneous* $T_F^{(2)}$*-branch (heavy) and heterogeneous branches (solid; dashed) corresponding with a parent solutions from each clusters of solutions. (Subscripts indicate associated wave-number groups.) The solid branches correspond with 1-mode and quasi 1-mode bifurcation solutions; the dashed branches correspond with true 2-mode bifurcation solutions.*

5.4 Heterogeneous solutions and higher dimensional nullspaces

In the case study above, 2-mode bifurcations occurred for wave-number groups $[(k,\ell),(\ell,k)]$, with $k \neq \ell$. This corresponds to a 2-dimensional nullspace of the Jacobian. In this section we

show, by way of example, that for certain parameter values it may happen that nullspaces (of the Jacobian) with dimension higher than two can occur. This then leads to m-mode bifurcation solutions with $m > 2$, which for increasing m have a stronger heterogenity.

An m-mode bifurcation point occurs if the following two conditions are satisfied. Firstly, there must be m distinct wave-number pairs (n_i, p_i), $1 \leq i \leq m$, that satisfy

$$\sqrt{n_1^2 + \left(\frac{p_1}{D_1}\right)^2} = \sqrt{n_2^2 + \left(\frac{p_2}{D_1}\right)^2} = \cdots = \sqrt{n_m^2 + \left(\frac{p_m}{D_1}\right)^2} = \kappa, \tag{59}$$

and, secondly, this constant κ should satisfy the inequality

$$\kappa\pi \tanh(\kappa\pi D_2) + \gamma_{min} \leq 0, \tag{60}$$

with $\gamma_{min} = \gamma(T_F)|_{\lambda=1}$ (cf. Section 5.2). Relation (60) ensures that there exists a $\lambda \in (0,1)$ such that (42) holds for $\zeta_{n_i,p_i} = 0$ and $\widetilde{W}_{n_i,p_i} \neq 0$, $i = 1, \ldots, m$. The corresponding m-mode bifurcation solution is of the form

$$T_F(x,y) = T_F^{(2)} + \epsilon \sum_{i=1}^{m} c_i \cos(n_i \pi x) \cos\left(\frac{p_i \pi y}{D_1}\right), \quad \epsilon \downarrow 0, \tag{61}$$

and is a generalisation of (44), (45).

As an example of a higher-degree ($m > 2$) bifurcation, we reconsider the case study of the square fluid-heater interface with a more flattened heater ($D_2 = 0.05$) and the remaining parameters unchanged. The wave-number pairs for which a bifurcation on the homogeneous $T_F^{(2)}$-branch occurs are represented schematically in Figure 14*a*. This shows that the flattening of the heater (by decreasing D_2) enlarges the set of bifurcations considerably (compare with Figure 7*a*). This configuration admits one bifurcation with four vanishing coefficients $\zeta_{k,l}$ (4-mode bifurcation) which involves the wave-number group $\{(0,5),(5,0),(3,4),(4,3)\}$. For all $(n_i, p_i) \in \{(0,5),(5,0),(3,4),(4,3)\}$ we have $\kappa = \sqrt{n_i^2 + p_i^2} = 5$, i.e. (59) holds with $D_1 = 1$ (square heater) and $m = 4$. Moreover, for $\kappa = 5$ and $D_2 = 0.05$ one can check that the inequality (60) holds. This 4-mode case clearly allows greater variation in solutions compared to lower degrees of multiplicity. However, similar to the 2-mode bifurcation solutions of the case study (Section 5.3), there are limitations w.r.t. the choice of the coefficients c_i that restrict the 4-mode bifurcation solutions to specific subspaces. We give a few examples of physically-meaningful solutions originating from admissible 4-mode bifurcation solutions. In Figure 14*b* and Figure 14*c* we show heterogeneous solutions corresponding with the 4-mode bifurcation solution (61) for $(c_1, c_2, c_3, c_4) = (0, 0, 1, 1)$ and $(c_1, c_2, c_3, c_4) = (0, 1, 0, 1)$. These are quasi 2-mode bifurcation solutions. Figure 14*d* shows the heterogeneous solution originating from (61) with $(c_1, c_2, c_3, c_4) = (1, 1, 1, 1)$. This is a true 4-mode solution, which has a more complex structure than solutions in the cases involving only two Fourier modes. The temperature range in Figure 14*d* is significantly narrower (minimum (blue): $T \approx 1$; maximum (red): $T \approx 1.4$) than for the heterogeneous solutions found before ($0.5 \lessapprox T \lessapprox 2$). This suggests that heterogeneous solutions of the pool-boiling problem attain, in the sense of both length scales and temperature fluctuations, progressively finer structures with increasing degree of multiplicity m.

The above discussion on higher dimensional nullspaces is by no means exhaustive and only gives a first impression of the intricate behaviour that may be encountered in the 3D pool-boiling problem. Further investigation is required to understand and explain the phenomena related to higher multiplicities.

6 Conclusions

In this paper we consider a 3D heat-transfer problem with a nonlinear Neumann boundary condition on part of the boundary as a simple model for 3D pool boiling processes. This model is the same as the one in the 2D pool-boiling problem studied in [18]. The heat flux from the heater to the fluid is modelled by means of a nonlinear functional relation between the local heat flux and the boundary temperature. A key issue is the existence of multiple steady-state solutions with heterogeneous temperature distributions on the fluid-heater interface. The separation-of-variables technique enables analytical reduction of the full 3D problem to a 2D problem for the temperature distribution on the fluid-heater interface (as in (11)). This reduced problem forms the basis of the analysis and is discretised using a Fourier collocation method. Both the continuous and discrete interface problems have symmetry properties (Theorem 2 and Remark 4) that imply multiplicity of heterogeneous solutions. These symmetries are direct consequences of the shift-invariance property (24). Multiple (heterogeneous) solutions originate from bifurcations on a branch of homogeneous solutions. *The existence of symmetries (Theorem 2) and the conservation of symmetries during continuation (Theorem 1) are two fundamental properties of the model.* The steady-state behaviour of the 3D pool-boiling model is studied through a numerical bifurcation analysis of the reduced problem and demonstrates the multiple solution structure by way of a representative case study. Below we outline a few main conclusions from this analysis.

Multiple (heterogeneous) steady-state solutions are found in systems that admit transition boiling modes; systems admitting only nucleate or film boiling allow only one unique and homogeneous solution. Heterogeneous solutions represent temperature distributions that correspond to coexisting nucleate and film boiling regions on the interface. Heterogeneous solutions emerge clusterwise from pitchfork bifurcations on the homogeneous solution branch in the transition regime. The occurrence of (multiple) heterogeneous solutions in the transition regime is consistent with results known from laboratory experiments. This suggests that the proposed model provides an (at least qualitatively) adequate description of 3D pool boiling.

The 3D pool-boiling model behaves to a large extent similar to the 2D model. The 2D and 3D problems share two key properties. Firstly, the shift-invariance property that underlies the fundamental multiplicity in steady-state solutions and secondly, bifurcations undergone by the homogeneous solution in the transition regime are the origin of multiple (heterogeneous) steady-state solutions. There is, however, also a fundamental difference. The 3D system admits bifurcations with multi-dimensional nullspaces; 2D systems, in contrast, admit only one-dimensional nullspaces. This leads to 3D solution structures that have no 2D counterpart. Numerical experiments suggest that the freedom within multi-dimensional nullspaces is restricted in that only specific heterogeneous solutions are allowed to emerge from the corresponding bifurcations. The underlying mechanism for this phenomenom is not yet understood.

Related to current and future research we note the following. Studies on the bifurcation behaviour associated with system parameters other than the artificial nonlinearity parameter considered here are in progress. Preliminary stability studies reveal that steady-state solutions are always unstable, except for a homogeneous solution each in the nucleate and film-boiling regimes. We are currently working on an analysis to explain this stability property. Further issues to be considered in future work may include the effect of different heating methods and stabilisation of pool-boiling processes via active control [1].

Acknowledgment

The presented work has benefitted greatly from the continuation algorithm kindly provided by Robert Grosch, Process Systems Engineering, RWTH Aachen. Moreover, one of us (MS) gratefully acknowledges financial support from the Deutsche Forschungsgemeinschaft (DFG) via the Research Training Group "Hierarchy and Symmetry in mathematical Models".

References

[1] Auracher, H. & Marquardt, W. 2002 Experimental studies of boiling mechanisms in all boiling regimes under steady-state and transient conditions. *Int. J. Therm. Sci.*, **41**,pp. 586-598.

[2] Auracher, H. & Marquardt, W. 2004 Heat transfer characteristics and mechanisms along entire boiling curves under steady-state and transient conditions. *J. Heat Fluid Flow*, **25**, pp. 223-242.

[3] Blum, J., Lüttich, T. & Marquardt, W. 1999 Temperature wave propagation as a route from nucleate to film boiling? In *Proceedings of the Second International Symposium on Two-Phase Flow Modelling and Experimentation, Rome, Vol 1* (ed. G.P. Celata, P. DiMarco & R.K. Shah), Edizioni ETS, Pisa.

[4] Canuto, C., Hussaini, M. Y., Quarteroni, A. & Zang, T. A. 1987 *Spectral Methods in Fluid Dynamics*. Springer, Berlin.

[5] Dhir, V. K. 1991 Nucleate and transition boiling heat transfer. *Int. J. Heat Fluid Flow*, **12**, pp. 290–314.

[6] Dhir, V. K. 1998 Boiling Heat Transfer. *Ann. Rev. Fluid Mech.* **30**, 365–401.

[7] Gabaraev, B. A., Kovalev, S. A., Molochnikov, Yu. S., Solov'ev, S. L. & Usitakov, S. V. 2001 Rewetting and autowave change of boiling modes. *High Temp.*, **39**, pp. 302-314.

[8] Gonzalez-Velasco, E. A. 1995 *Fourier Analysis and Boundary Value Problems*. Academic Press, San Diego.

[9] Govaerts, W. J. F 2000 *Numerical Methods for Bifurcations of Dynamical Equilibria*, SIAM, Philadelphia.

[10] Kovalev, S. A. 1966 An investigation of minimum heat fluxes in pool boiling of water. *Int. J. Heat Mass Transfer*, **9**, pp. 1219-1226.

[11] Kovalev, S. A. & Rybchinskaya, G. B. 1978 Prediction of the stability of pool boiling heat transfer to finite disturbances. *Int. J. Heat Mass Transfer*, **21**, pp. 691-700.

[12] Kovalev, S. A. & Usitakov, S. V. 2003 Analysis of the stability of boiling modes involving the use of stability diagrams. *High Temp.*, **41**, pp. 68-78.

[13] Kreyszig, E. 1999 *Advanced Engineering Mathematics*, Wiley, Chichester.

[14] Mudawar, I. 2001 Assessment of High-Heat-Flux Thermal Management Schemes. *IEEE Transactions-CPMT: Components and Packaging Technologies*, **24**, pp. 122-141.

[15] Ott, E. 2002 *Chaos in Dynamical Systems*. Cambridge University Press, Cambridge (second edition).

[16] van Ouwekerk, H. 1972 Burnout in pool boiling. The stability of boiling mechanisms. *Int. J. Heat Mass Transfer*, **15**, pp. 25–33.

[17] Speetjens, M. F. M. 2005 Steady-state behaviour of 2D pool-boiling problems. In *Proceedings Eurotherm seminar 82 Numerical Heat Transfer* (ed. A. J. Nowak, R. A. Bialecki & G. Wecel).

[18] Speetjens, M., Reusken, A. & Marquardt, W. 2006 Steady state solutions in a nonlinear pool-boiling heat transfer model. *IGPM report 256, RWTH Aachen.* Submitted to *Communications in Nonlinear Science and Numerical Simulation*

[19] Theofanous, T. G.. Tu, J. P., Dinh, A. T. & Dinh, T. N. 2002 The boiling crisis phenomenon. Part I: nucleation and nucleate boiling heat transfer. *Exp. Therm. Fluid Sci.*, **26**, pp. 775–792.

[20] Thome, J.R. 2003 Boiling. In *Handbook of Heat Transfer* (ed. A. Bejan & A. D. Krause), Wiley & Sons, Hoboken, pp 635-717.

[21] Zhukov, S. A., Barelko, V. V. & Merzhanov, A. G. 1980 Wave processes on heat generating surfaces in pool boiling. *Int. J. Heat Mass Transfer*, **24**, pp. 47-55.

[22] Zhukov, S. A. & Barelko, V. V. 1983 Nonuniform steady states of the boiling process in the transition region between the nucleate and film regimes. *Int. J. Heat Mass Transfer*, **26**, pp. 1121-1130.

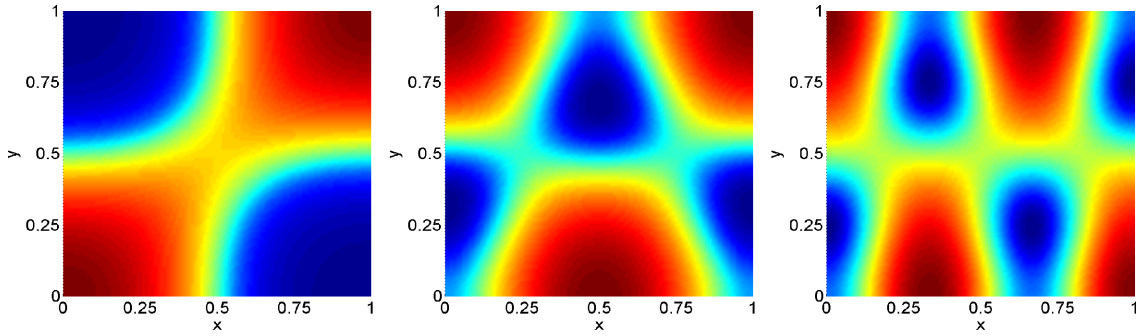

a) T_F *for* $k = 1$. *b)* T_F *for* $(k, \ell) = (2, 1)$ *c)* T_F *for* $(k, \ell) = (3, 1)$

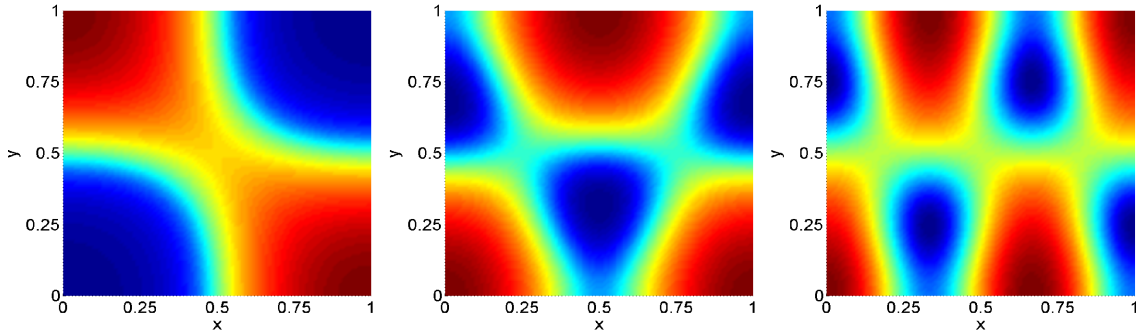

d) T_F^* *for* $k = 1$. *e)* T_F^* *for* $(k, \ell) = (2, 1)$. *f)* T_F^* *for* $(k, \ell) = (3, 1)$.

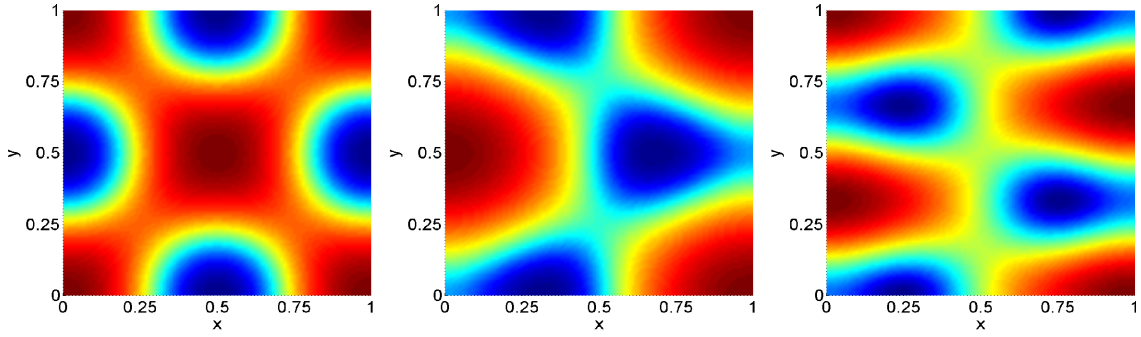

g) T_F *for* $k = 2$. *h)* T_F' *for* $(k, \ell) = (2, 1)$. *i)* T_F' *for* $(k, \ell) = (3, 1)$.

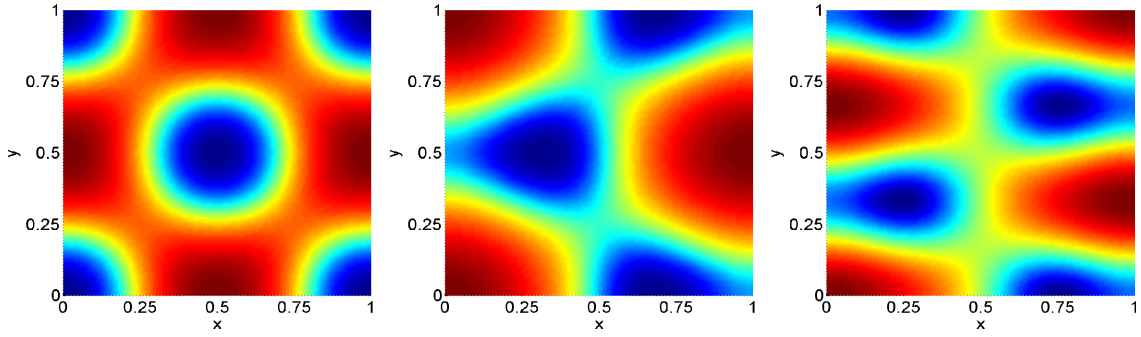

j) T_F^* *for* $k = 2$. *k)* $T_F^{*\prime}$ *for* $(k, \ell) = (2, 1)$. *l)* $T_F^{*\prime}$ *for* $(k, \ell) = (3, 1)$.

Figure 12: *Physically-meaningful* ($\lambda = 1$) *solutions corresponding with 1-mode bifurcation solutions* (44) *for* $k = 1$ *and* $k = 2$. *The remaining columns give the cluster of 4 solutions* (51) *emerging from quasi 1-mode bifurcation for* $(k, \ell) \in \{(1, 2), (2, 1)\}$ *(second column) and* $(k, \ell) \in \{(1, 3), (3, 1)\}$ *(third column).*

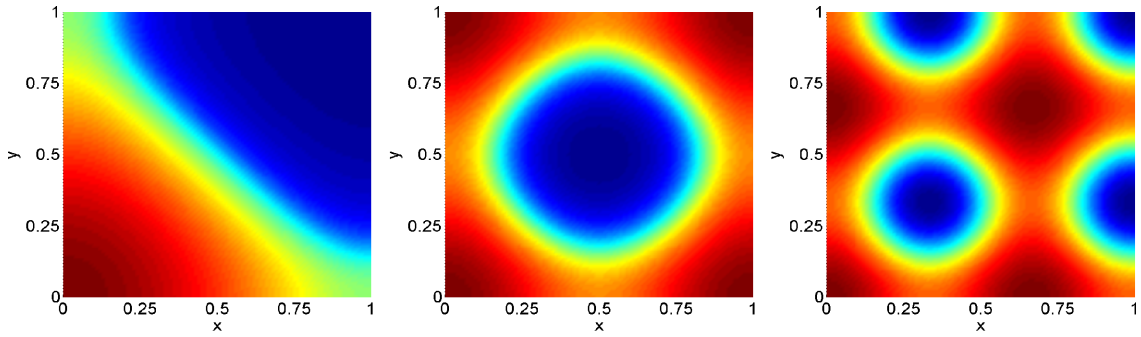

a) T_F *for* $(k,\ell) = (1,0)$. *b)* T_F *for* $(k,\ell) = (2,0)$. *c)* T_F *for* $(k,\ell) = (3,0)$.

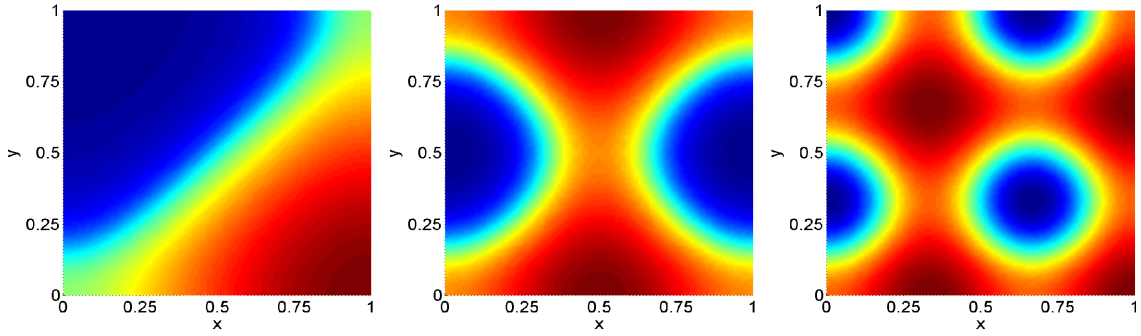

d) $T_F^{*,1}$ *for* $(k,\ell) = (1,0)$. *e)* $T_F^{*,1}$ *for* $(k,\ell) = (2,0)$. *f)* $T_F^{*,1}$ *for* $(k,\ell) = (3,0)$.

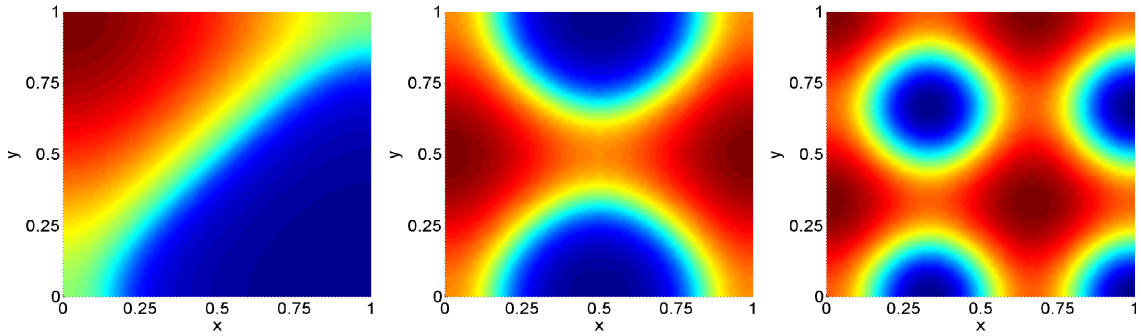

g) $T_F^{*,2}$ *for* $(k,\ell) = (1,0)$. *h)* $T_F^{*,2}$ *for* $(k,\ell) = (2,0)$. *i)* $T_F^{*,2}$ *for* $(k,\ell) = (3,0)$.

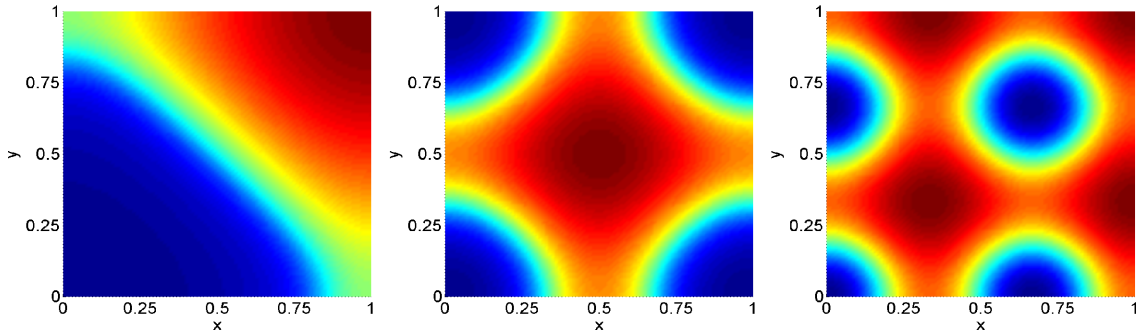

j) $T_F^{*,3}$ *for* $(k,\ell) = (1,0)$. *k)* $T_F^{*,3}$ *for* $(k,\ell) = (2,0)$. *l)* $T_F^{*,3}$ *for* $(k,\ell) = (3,0)$.

Figure 13: *Physically-meaningful* ($\lambda = 1$) *cluster of true 2-mode solutions emerging from the 2-mode bifurcation solutions* (56) *for* $\ell = 0, k = 1, 2, 3$.

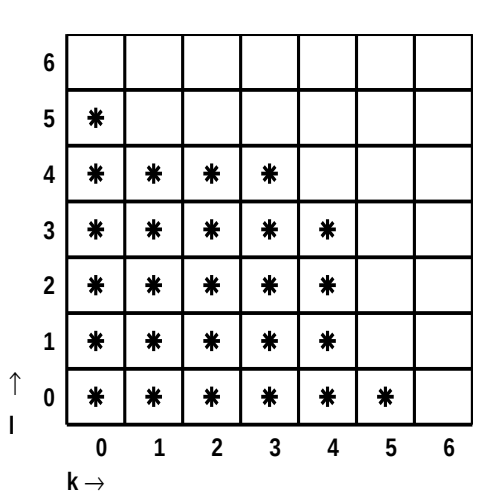

a) Bifurcations.

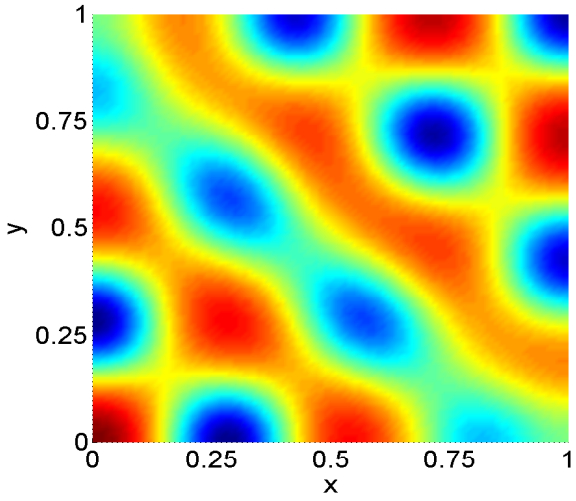

b) T_F for $c_1 = c_2 = 0$, $c_3 = c_4 = 1$.

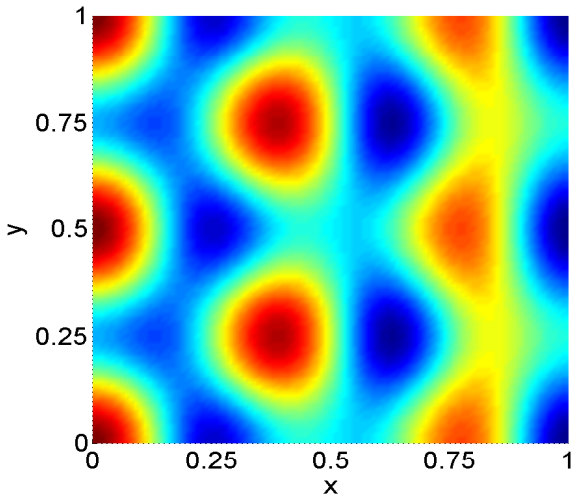

c) T_F for $c_2 = c_4 = 1$, $c_1 = c_3 = 0$.

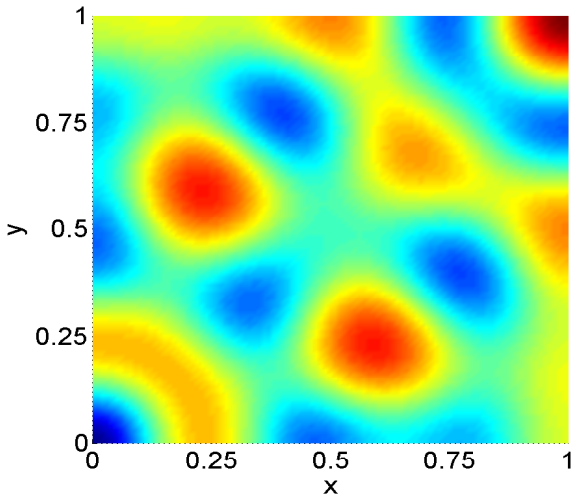

d) T_F for $c_1 = c_2 = c_3 = c_4 = 1$.

Figure 14: *Heterogeneous solutions for the flattened square heater ($D_2 = 0.05$). Panel a gives the wave-number pairs for which bifurcations on the homogeneous $T_F^{(2)}$-branch occur. Panels b-d give a few physically-meaningful ($\lambda = 1$) solutions T_F originating from* (61) *for coefficients c_i as indicated.*